Drug Design, Development and Therapy

Dovepress
Taylor & Francis Group

Open Access Full Text Article

ORIGINAL RESEARCH

Lobetyolin Suppressed Osteoclastogenesis and Alleviated Bone Loss in Ovariectomy-Induced Osteoporosis via Hindering p50/p65 Nuclear Translocation and Downstream NFATc1/c-Fos Expression

Chunmei Xiu[1,2,*], Hua Luo[3,*], Weixing Huang[4,5,*], Shaohua Fan[3], Chiting Yuan[3], Jiangjie Chen[3], Chenghao Xu[3], Can Yao[3], Dun Hong[1,3], Liwei Zhang[1,3]

[1]Institute of Bone Metabolism, Taizhou Hospital of Zhejiang Province, School of Medicine, Zhejiang University, Taizhou, 317000, People's Republic of China; [2]Department of Clinical Medicine, Key Laboratory of Novel Targets and Drug Study for Neural Repair of Zhejiang Province, School of Medicine, Hangzhou City University, Hangzhou, 310015, People's Republic of China; [3]Orthopedic Department, Taizhou Hospital of Zhejiang Province, School of Medicine, Zhejiang University, Taizhou, 317000, People's Republic of China; [4]General Surgical Department, Taizhou Hospital of Zhejiang Province, School of Medicine, Zhejiang University, Taizhou, 317000, People's Republic of China; [5]Department of Nursing, Zhejiang University School of Medicine First Affiliated Hospital, School of Medicine, Zhejiang University, Hangzhou, 310000, People's Republic of China

*These authors contributed equally to this work

Correspondence: Liwei Zhang; Dun Hong, Email medzlw@sina.com; hongd@enzemed.com

Purpose: To investigate the therapeutic potential of lobetyolin (LBT), a bioactive compound derived from *Codonopsis pilosula*, against bone loss in postmenopausal osteoporosis (PMOP).

Methods: To investigate the therapeutic potential of LBT in osteoporosis, a multifaceted approach involving network pharmacology and molecular docking was employed to identify relevant targets and elucidate mechanisms of action. In vitro experiments evaluated LBT's impact on osteoclastogenesis, bone resorption, and osteoblast differentiation using bone marrow macrophages (BMMs) and bone marrow mesenchymal stromal cells (BMSCs). The inhibition of RANKL-activated NF-κB signaling and downstream NFATc1/c-Fos pathways was analyzed via Western blot and immunofluorescence. Additionally, an in vivo ovariectomy (OVX)-induced osteoporosis mouse model was utilized to examine the effects of LBT on bone architecture, assessed through micro-CT imaging and histological analyses.

Results: LBT effectively suppressed RANKL-driven osteoclast differentiation in vitro without cytotoxic effects, reducing osteoclast numbers, size, and resorptive function. It also downregulated osteoclast-specific genes expressions, inhibited ROS production, and disrupted the NF-κB signaling cascade by blocking p50/p65 nuclear translocation. Moreover, LBT mitigated LPS-induced osteogenic impairment, enhancing osteoblast differentiation and mineralization. In the OVX mouse model, LBT treatment improved bone microstructure. Histological analyses further corroborated LBT's role in reducing osteoclast activity and promoting bone formation.

Conclusion: LBT exerts a dual effect on bone remodeling, simultaneously inhibiting osteoclast-mediated bone resorption and promoting osteoblast-driven bone formation. By targeting key pathways such as NF-κB/NFATc1/c-Fos and reducing inflammatory responses, LBT emerges as a potential therapeutic agent for managing PMOP and other conditions associated with excessive bone loss, offering a safer alternative to current treatments.

Keywords: postmenopausal osteoporosis, osteoclast, lobetyolin, inflammation, osteoblast

Introduction

Osteoporosis is a degenerative skeletal disease characterized by a reduction in bone mineral density (BMD) and the breakdown of bone micro-architecture. Postmenopausal osteoporosis (PMOP), also known as primary osteoporosis type I, arises

Received: 22 January 2025
Accepted: 24 May 2025
Published: 3 June 2025

Graphical Abstract

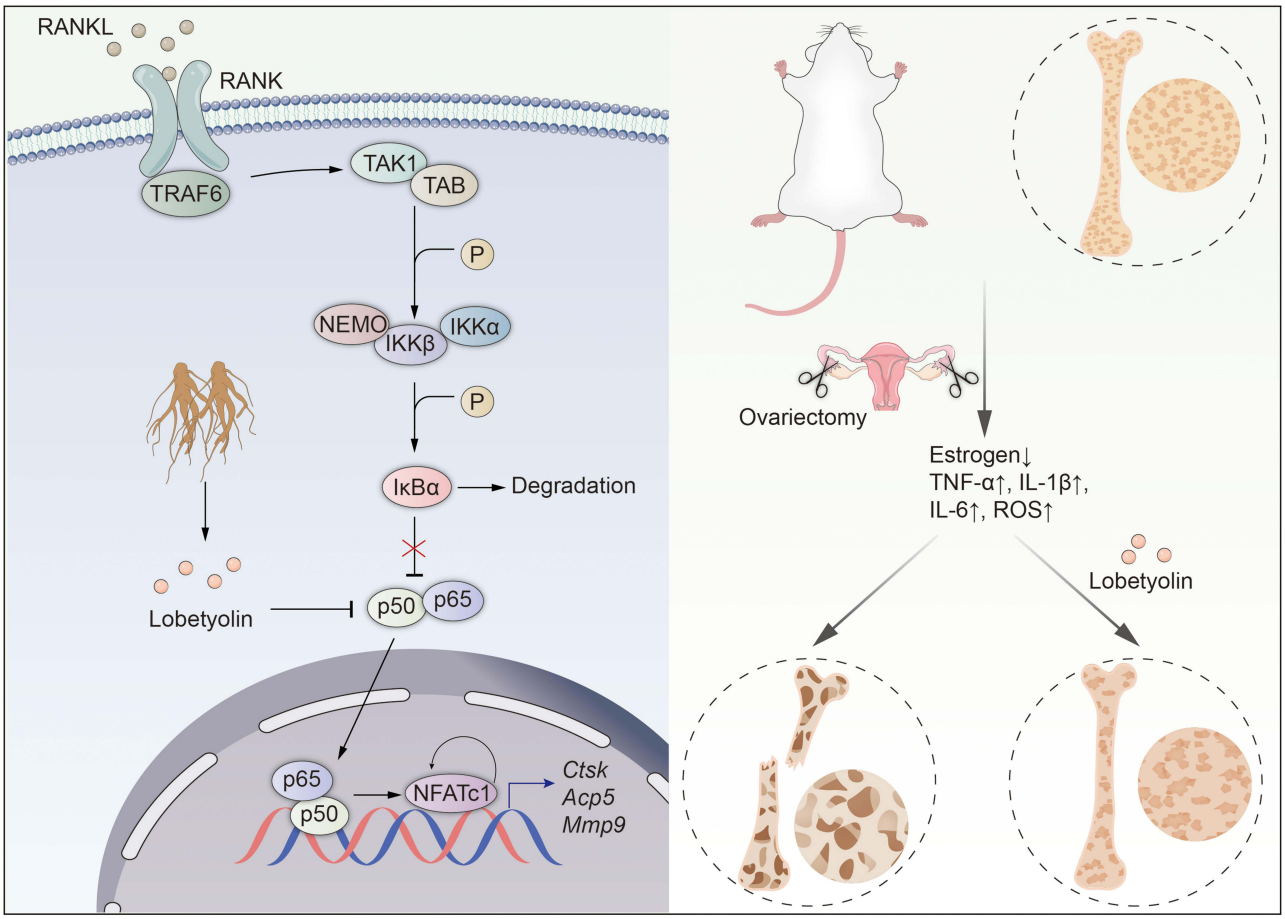

from a steady decline in estrogen levels after menopause, leading to significant bone loss.[1] Skeletal health relies on the dynamic balance of bone remodeling, where osteoclast-mediated bone resorption and osteoblast-driven bone formation are synchronized in a spatial and temporal manner. Osteoclasts (OCs) are specialized, multinucleated cells that specifically originate from bone marrow monocytes/macrophages (BMMs) to resorb bone tissue. Meanwhile, osteoblasts (OBs) that were derived from bone marrow mesenchymal stromal cells (BMSCs), play a central role in bone formation, structural maintenance, and mineralization of the bone matrix.[2] Endocrine factors like parathyroid hormone and estrogen play vital roles in regulating osteoblast and osteoclast function. Estrogen deficiency has been widely recognized as a key factor in PMOP progression with the effect of disrupting bone remodeling balance and leading to bone loss. Furthermore, chronic inflammation exacerbated by estrogen deficiency promotes the release of pro-inflammatory cytokines that enhance osteoclast activity and impede bone formation.[3–5]

Currently, bisphosphonates, denosumab, and teriparatide combined with daily adequate vitamin D and calcium intake are effective treatment means in inhibiting osteoclastogenesis or promoting bone formation.[6,7] Besides, as a biological agent by inhibiting sclerostin that normally suppresses bone formation, romosozumab shows remarkable effect both in promoting bone formation and hindering bone resorption.[8] Recently, our team has identified the anti-porosis effect and underlying mechanism of Hedgehog signaling, protein S-palmitoylation, and monomer agents including bulleyaconitine A and MCC950.[9–12] However, long-term use of high oral doses may lead to several adverse effects, including gastrointestinal discomfort, renal function abnormalities, cardiovascular event, and an increased risk of breast cancer.

To simulate the pathological process of postmenopausal osteoporosis, ovariectomy (OVX) operation was reported to induce chronic inflammation in the bone marrow.[13–15] Recent researches have increasingly highlighted the critical role of anti-inflammatory drugs in bone health. For instance, a cytokine-suppressive and non-steroidal anti-inflammatory drug benzydamine has been uncovered the capacity in inhibiting osteoclast formation and promoting osteoblast differentiation via hindering nuclear factor-κB (NF-κB) activation and IL-1β expression.[16] Targeting inflammatory signal pathway, a series of drugs including alloferon-1, catalpol, and tussilagone have been identified the effect of alleviating bone loss.[17–19] Lobetyolin (LBT), a biologically active compound extracted from *Codonopsis pilosula*, is recognized for its anti-inflammatory properties, likely mediated through inhibition of pro-inflammatory cytokines and suppression of oxidative stress pathways.[20,21] These effects are critical in bone metabolism, as chronic inflammation and oxidative stress disrupt the balance between osteoblast-mediated bone formation and osteoclast-mediated bone resorption. Recently, we revealed that LBT exhibited effective bio-activity in suppressing osteoclastogenesis and reduce inflammation level, leading to alleviating bone loss in ovariectomy-induced osteoporosis.

Materials and Methods

Network Pharmacology Analysis

Identification of Lobetyolin-Targeted Genes

Genes targeted by LBT were obtained from the online databases SuperPred and Swiss Target Prediction using "lobetyolin" as the search keyword.[22,23] Targets with probability values above 0.1 were selected as active component targets. The results from the two databases were combined, and duplicate entries were removed to identify the unique targets of LBT. We used UniProt ID mapping tools to convert the LBT target proteins into their corresponding gene symbols.

Identification of Osteoporosis-Related Genes

The genes related to *osteoporosis* were obtained from GeneCards databases. The search term in this work was "osteoporosis". Targets larger than the median of relevance score were selected.[24] Similarly, we convert the LBT target proteins into their corresponding gene symbols via UniProt ID mapping tools. Then, we obtained the intersection of gene targets of LBT and osteoporosis using bioinformatics online platform (https://www.bioinformatics.com.cn/).

Enrichment Analysis of the Intersected Genes

To gain insight into the functions of the intersecting targets, gene ontology (GO) and Kyoto encyclopedia of genes and genomes (KEGG) pathway enrichment analyses were performed using the DAVID database. GO terms and KEGG pathways with p-values below 0.05 were regarded as significantly enriched. Top 20 KEGG pathways and GO terms were initially ranked by based on the lowest p values to prioritize those with the strongest statistical evidence of enrichment.[25] The pathway enrichment analysis results were visualized through bioinformatics online platform.

Construction of the Drug-Ingredient-Target Network and Protein-Protein Interactions

To elucidate the mechanisms by which LBT combats osteoporosis, a network including integrating components, disease-related targets, and pathways was developed using Cytoscape software (version 3.9.1). Additionally, the shared targets of LBT for treating osteoporosis were input into the STRING database, allowing us to generate comprehensive predicted protein-protein interaction (PPI) networks and associated data to forecast these interactions.

Molecular Docking

The identified key genes were selected as primary receptor targets, with receptor structure data sourced from the PDB and UniProt databases. The molecular structure of LBT was retrieved from the PubChem database, and optimized ligands were utilized as initial inputs for docking. Protein-ligand molecular docking and associated calculations were carried out using CB-DOCK2. Upon completion of the docking analysis, the conformations and minimum binding energies of ligand-receptor interactions were obtained. To validate our docking protocol, we incorporated a well-characterized p50 inhibitor (andrographolide) as a positive control. The docking procedure was repeated for this compound using the same

parameters applied to LBT. The predicted binding pose and affinity of andrographolide aligned closely with published binding data, confirming the reliability of our docking protocol.[26]

This research has been conducted using the public databases involving human data and approved by the Ethics Committee of the Taizhou Hospital of Zhejiang Province (tzyy-2022007).

Reagents and Animals

Lobetyolin (#HY-N0327, LBT) was purchased from MedChemExpress (Monmouth Junction, NJ, USA) and dissolved in DMSO (#ST038, Beyotime Biotechnology, Shanghai, China) with a concentration of 100 mm. RIPA buffer (#P0013B), phenylmethanesulfonyl fluoride (PMSF, #ST505), phosphatase inhibitor cocktail (#P1081), lipopolysaccharide (LPS, #S1732), penicillin/streptomycin (#C0222), Reactive Oxygen Species Assay Kit (#S0033), and 2.5% trypsin (#C0201) were obtained from Beyotime Biotechnology (Shanghai, China). The α-minimum essential medium (#SH30265.01, α-MEM) and Dulbecco's phosphate-buffered saline (#SH30028.02, DPBS) were supplied by Hyclone (Logan, UT, USA). Fetal bovine serum (#10099141, FBS) was obtained from Gibco-BRL (Waltham, MA, USA). Recombinant mouse macrophage-colony stimulating factor (#P00107, M-CSF), recombinant receptor activator for nuclear factor-κB ligand (#P02067, RANKL), and red blood cell lysis buffer (#R1010) were purchased from Solarbio Life Science (Beijing, China). Cell counting kit-8 (#R22305, CCK-8), dexamethasone (#S17003), and L-ascorbic acid (#S13001) were supplied by Yuanye Bio-Technology (Shanghai, China). β-glycerophosphate (#G5422) was obtained from Sigma-Aldrich (St. Louis, MO, USA). Rabbit primary antibodies against p-p65 (#3033, 1:1000), AKT (#9272, 1:1000), p-AKT (#9271, 1:1000), JNK (#9252, 1:1000), p-JNK (#4668, 1:1000), p38 (#8690, 1:1000), ERK (#4695, 1:1000), p-ERK (#4370, 1:1000), and β-Actin (#4970, 1:2000) were obtained from Cell Signaling Technology (Cambridge, MA, USA). Rabbit primary antibodies for p-p38 (#ab4822, 1:1000), NFATc1 (#ab25916, 1:1000), and c-Fos (#ab190289, 1:1000) were purchased from Abcam (San Francisco, CA, USA). Rabbit primary antibodies against total p65 (#10745-1-AP, 1:1000), GAPDH (#10494-1-AP, 1:2000), Histone H3 (#17168-1-AP, 1:2000), and CoraLite® Plus 594-Goat anti-rabbit recombinant secondary antibody (#RGAR004, 1:1000) were purchased from Proteintech (Wuhan, Hubei, China). HRP-conjugated anti-rabbit secondary antibody (#D110058, 1:2000) was provided by Sangon Biotech (Shanghai, China).

The C57BL/6 mouse were obtained from SLAC laboratory animal (Shanghai, China). All experimental operations involving animal were followed the NIH Guide for the care and use of laboratory animals and approved by the Ethics Committee of the Taizhou Hospital of Zhejiang Province (tzyy-2022007). All animals were kept in a specific pathogen-free (SPF) facility under controlled conditions, including a 12-hour light/dark cycle and a stable temperature of 22 ± 1 °C.

Cell Culture and Differentiation

BMMs were extracted from the femurs and tibiae of 6- to 8-week-old mouse and cultured in complete α-MEM medium supplemented with 10% FBS and 30 ng/mL M-CSF for 24 h following erythrocyte lysis. After the medium was discarded, the cells were rinsed twice with DPBS and maintained in fresh medium for an additional 2 d until they reached 90% confluence. To induce osteoclast formation, BMMs were further seeded onto tissue culture treated plate at a density of 6×10^4 cells/cm² and stimulated with 30 ng/mL M-CSF and 50 ng/mL RANKL.

Similarly, BMSCs were isolated from the femurs and tibiae of 6- to 8-week-old mouse and initially cultured in complete α-MEM medium containing 10% FBS for 3 d after erythrocyte lysis. The medium was then replaced, and the cells were washed twice with DPBS before being cultured in fresh medium for another 3 d until 90% confluence was achieved. To induce osteoblast differentiation, BMSCs were seeded onto tissue culture treated plate at a density of 6×10^4 cells/cm² and treated with 50 μg/mL L-ascorbic acid, 10 mm β-glycerophosphate, and 100 nM dexamethasone. All cell cultures were maintained in a humidified incubator at 37 °C with 5% CO_2.

Cell Viability

Cell counting kit-8 was employed to evaluate the cytotoxic effects of LBT on the proliferation of BMMs and BMSCs. Actively growing cells were seeded in a 96-well plate at a density of 5000 (BMMs) or 8000 (BMSCs) cells per well, with six replicates for each condition. After 24 h, the cells were treated with either a vehicle control (DMSO) or varying concentrations of LBT for 48, 72, and 96 h. At each time point, cells were cultured for 2 h at 37 °C after addition of

10 μL CCK-8 reagent to each well. Absorbance was measured at 450 nm by Multiskan™ FC Microplate Photometer (Thermo Fisher Scientific, Waltham, MA, USA).

To further confirm the toxicity of LBT on BMMs, Calcein/PI Cell Viability/Cytotoxicity Assay Kit (#C2015, Beyotime Biotechnology, Shanghai, China) was applied according specification. Briefly, calcein AM is a non-fluorescent compound that becomes fluorescent only after entering viable cells, where it is cleaved by active intracellular esterases to generate calcein. This resulting molecule is highly polar and negatively charged, preventing it from crossing the cell membrane and causing it to accumulate inside the cell. Calcein emits a strong green fluorescence, serving as an indicator of cell viability. In contrast, dead cells, which lack esterase activity or have it significantly reduced, produce little to no calcein, leading to negligible fluorescence. Meanwhile, propidium iodide (PI), a red fluorescent nucleic acid stain, cannot permeate the intact membranes of live cells but readily penetrates compromised membranes in dead cells, selectively marking them with red fluorescence.

TRAP Staining

Osteoclasts were rinsed twice with PBS and fixed in 4% paraformaldehyde (PFA, #G1101, Servicebio, Wuhan, Hubei, China) for 10 min at room temperature (RT). Following two additional PBS washes, the cells were incubated at 37 °C for 20 min in a substrate solution containing L-(+) tartaric acid (#1291074-87-7, Yuanye Bio-Technology, Shanghai, China) and naphthol AS-BI phosphate (#A606682, Sangon Biotech, Shanghai, China). Subsequently, they were treated with a color-developing solution consisting of sodium nitrite (#A415326, Sangon Biotech, Shanghai, China) and pararosaniline chloride (#S19024, Yuanye Bio-Technology, Shanghai, China), incubating for 20 min in the dark. TRAP staining images were captured using the IXplore standard compound microscope system and the BX43 manual system microscope (Olympus Corporation, Tokyo, Japan). The area of TRAP-positive cells (with $\geq$ 3 nuclei) was quantified using ImageJ software (National Institutes of Health, Bethesda, MD, USA).

Podosome Fluorescence Staining

To visualize the podosome which was dynamic and filamentous actin (F-actin) structure specifically in osteoclast, cells were labeled with phalloidin, a fluorescent probe that specifically binded to polymerized actin. Firstly, the cells were fixed in 4% PFA at RT for 10 min, followed by permeabilization with 0.1% Triton X-100 (#GC204003, Servicebio, Wuhan, Hubei, China). To block nonspecific binding, the cells were treated with 3% bovine serum albumin (BSA, #GC305010, Servicebio, Wuhan, Hubei, China) for 20 min. Subsequently, FITC-conjugated phalloidin (#MF8203, MesGen Biotech, Shanghai, China) was applied in a dark environment for 20 min to stain the actin filaments. Afterward, the nuclei were counterstained with 4′,6-diamidino-2-phenylindole dihydrochloride (DAPI, #MG1789, MesGen Biotech, Shanghai, China) for 5 min, and the samples were mounted using anti-fade medium (#MFF1002, MesGen Biotech, Shanghai, China). Fluorescence imaging of phalloidin was performed using the IXplore standard compound microscope system (Olympus Corporation, Tokyo, Japan). The number and relative size of phalloidin in each group were analyzed using ImageJ software.

Bone Resorption Assay

To evaluate the effect of LBT on the bone resorption capacity of osteoclast, sterile bovine bone slices were utilized as a substrate for osteoclast adhesion. The slices were initially immersed in 75% ethanol for 2 d to ensure sterility. Following this, they were thoroughly rinsed with PBS for 24 h, air-dried, and subsequently soaked in PBS for further use. BMMs were seeded into 6-well plates at a density of 2×10^4 cells/cm^2 cultured in osteoclastogenic medium for 3 d to induce the formation of small, fused immature osteoclasts. These cells were then detached using trypsin and reseeded onto the pre-treated bone slices placed in 96-well plates at the same density. The cells were cultured in osteoclast differentiation medium containing 0, 10, or 20 μM LBT until they differentiated into mature, enlarged osteoclasts. Afterward, the bone slices were immersed in double-distilled water (ddH_2O) for 30 min and gently brushed to remove any remaining adherent cells. Finally, the slices were air-dried, coated with gold, and examined using a Hitachi S-4800 Field Emission Scanning Electron Microscope (SEM, Tokyo, Japan). The number of osteoclasts and the resorption area were quantified using ImageJ software.

Reactive Oxygen Species (ROS) Assay

To detect ROS generation, cells were labeled with DCFH-DA, a non-fluorescent compound readily traverses the cell membrane. Inside the cell, it undergoes hydrolysis by esterases, resulting in the formation of DCFH. ROS present in the cytoplasm oxidize DCFH, converting it into the fluorescent molecule DCF. BMMs were treated with 30 ng/mL M-CSF, 50 ng/mL RANKL, and 0, 10, and 20 μM LBT for 4 d. Then the cells were subjected to ROS examination according to the instruction manual. Fluorescence imaging of ROS was performed using the IXplore standard compound microscope system (Olympus Corporation, Tokyo, Japan).

Quantitative Reverse Transcription-Polymerase Chain Reaction (qRT-PCR)

After being cultured in differentiation medium with or without LBT, cells underwent total RNA extraction using the TRIzol reagent (#CW0580, Cwbiotech, Beijing, China) according to the manufacturer's protocol. The total RNA was then reverse-transcribed into cDNA using the 1st Strand cDNA Synthesis Kit (#E042, Novoprotein, Suzhou, Jiangsu, China). Quantitative real-time PCR (qPCR) was carried out on an ABI 7500 Real-Time PCR System (Applied Biosystems, Foster City, CA, USA) using Fast SYBR qPCR SuperMix (#E301, Novoprotein, Suzhou, Jiangsu, China). Reactions were performed in triplicate under the following conditions: 40 cycles of 94 °C for 30s, 60 °C for 10s, and 72 °C for 30s. Gene expression levels were normalized to the housekeeping gene GAPDH, and primer sequences are provided in Supplementary Table S1.

Western Blot

The total protein from each cell was extracted using RIPA buffer supplemented with the protease inhibitor PMSF and phosphatase inhibitor cocktail. Cytoplasmic and nuclear protein fractions were prepared following the protocol provided by the Nuclear and Cytoplasmic Protein Extraction Kit (#P0028, Beyotime Biotechnology, Shanghai, China). Protein concentrations were quantified with the BCA protein assay kit (#P0012, Beyotime Biotechnology, Shanghai, China). The absorbance at 562 nm (OD_{562}) was recorded using a Multiskan^{TM} FC microplate photometer (Thermo Fisher Scientific, Waltham, MA, USA). Samples were then combined with SDS-PAGE loading buffer (#P0015, Beyotime Biotechnology, Shanghai, China) and heated to 100 °C for 5 min. Equal amounts of protein were separated on 10% SDS-PAGE gels and transferred onto PVDF membranes (#ISEQ00010, Merck Millipore, Billerica, MA, USA). The membranes were blocked for 1 h with 5% non-fat milk (#A600669, Sangon Biotech, Shanghai, China) prepared in 1 × TBST, followed by overnight incubation at 4 °C with specific primary antibodies. Subsequently, the membranes were treated for 1 h at RT with HRP-conjugated secondary antibodies. Detection of immunoreactivity was performed using Chemiluminescent HRP Substrate (Millipore Corporation, Billerica, MA, USA) and captured with the ImageQuant LAS 500 system (GE Health Care, Fairfield, CT, USA). Band intensities were analyzed using ImageJ software.

Alkaline Phosphatase (ALP) Staining and Von Kossa Staining

For osteoblast differentiation assays, BMSCs were seeded into 12-well plates containing complete medium. Once the cells reached confluence, they were treated with osteogenic induction medium as previously described, along with or without LPS and LBT. To evaluate alkaline phosphatase activity, an ALP staining kit (#P0321, Beyotime Biotechnology, Shanghai, China) was employed. After being rinsed with DPBS, the cells were fixed in 4% PFA for 10 min, followed by incubation in an ALP staining solution prepared according to the manufacturer's instructions.

Mineralized nodule formation by mature osteoblasts was assessed using Von Kossa staining. In brief, the cells were fixed with 4% PFA for 10 min, washed with deionized water, and stained using a Von Kossa staining kit (#MVK1206, MesGen Biotech, Shanghai, China) in accordance with the provided protocol.

Ovariectomy (OVX)-Induced Osteoporosis Model Establishment and Analysis

After a one-week acclimation period, 18 female C57BL/6 mice, 8 weeks old, were randomly divided into three groups: sham-operated (Sham, n = 6), bilateral ovariectomy (OVX, n = 6), and OVX combined with LBT treatment (OVX + LBT, n = 6) using a computer-generated random number table to ensure unbiased allocation. Body weight was measured subsequent to group assignment, and no statistically significant differences were observed between

groups, confirming homogeneity. The mice were anesthetized via intraperitoneal injection of pentobarbital sodium (50 mg/kg) before undergoing bilateral ovariectomy (OVX and OVX + LBT groups) or partial removal of fat tissue near the ovaries (Sham group). Three days after surgery, the Sham and OVX groups received daily intraperitoneal injections of a vehicle solution (10% DMSO, 40% PEG300, and 5% Tween-80), while the OVX + LBT group was administered 20 mg/kg LBT in the same vehicle solution for 5 weeks. Selecting the 20 mg/kg dose of LBT for in vivo studies was based on the literature-based reference and in vitro results in this study.[27,28] The LBT dosage was selected based on prior research demonstrating its safety and effectiveness in mice at this concentration.[29] For the dynamic histomorphometric assessment, mice were administered intraperitoneal injections of calcein (10 mg/kg, #C0875, Sigma-Aldrich, St. Louis, MO, USA) on day 7 and 2 prior to euthanasia. At the end of the experimental period, following 8 h of fasting, the mice were anesthetized and euthanized. Samples, including serum tibias, and femurs, were collected, with serum stored at −80 °C and others fixed in 4% PFA for histological and micro-CT analysis.

Micro-Computed Tomography (μCT) Scanning

The distal femurs were scanned at a resolution of 9 μm per layer, with X-ray energy parameters set to 50 kV and 500 μA, and a rotational step of 0.7° per angle. Cross-sectional images were reconstructed using NRecon Software (SkyScan, Aartselaar, Belgium), while datasets were inspected and aligned with DataViewer (SkyScan, Aartselaar, Belgium). The region of interest (ROI) encompassed the distal femur and the upper edge of the growth plate. A total of 100 layers within the ROI were merged to create a volume of interest (VOI). Structural parameters of the cancellous bone and 3D images were analyzed with CTAn software (SkyScan, Aartselaar, Belgium), while Mimics software (Materialise, Leuven, Belgium) was used to generate stereoscopic reconstructions.

Histomorphometric Analysis

Bone samples were decalcified in 10% ethylenediaminetetraacetic acid (EDTA, #A100322, Sangon Biotech, Shanghai, China) for 14 d, followed by dehydration through a graded ethanol series and embedding in paraffin wax. Cross-sections of 6 μm thickness were prepared using a microtome (Leica Biosystems, Buffalo Grove, IL, USA). The sections were stained with hematoxylin and eosin (H&E) (#C0105, Beyotime Biotechnology, Shanghai, China) and TRAP (#MCP9580, MesGen Biotech, Shanghai, China) according to the manufacturer's protocols. Images of the stained samples were captured using a high-resolution microscope (Olympus, Japan). Osteoclast-related parameters, such as the number of osteoclasts per bone perimeter (N.Oc/BS) and osteoclast surface area per bone surface (Oc.S/BS), were quantified from the trabecular bone in the distal femur metaphysis using Bioquant II software (Bioquant Image Analysis Corp., Nashville, TN, USA).

Dynamic Histomorphometry

Undecalcified tibial sections were prepared using a modified tape transfer method as previously described.[30] The slides were rinsed with PBS, stained with DAPI, and mounted using anti-fade mounting medium. Fluorescent images were captured with a IXplore standard compound microscope system (Olympus Corporation, Tokyo, Japan). Parameters related to dynamic bone histomorphometry, including mineral apposition rate (MAR), and mineralizing surface percentage (MS/BS) were analyzed using Bioquant II software.

Enzyme Linked Immunosorbent Assay (ELISA)

To assess the impact of LBT treatment on bone resorption and formation in mice, we first prepared serum samples. The levels of carboxy-terminal cross-linked telopeptide of type 1 collagen (CTX-1) and osteocalcin (OCN) in the serum were then measured, following the method outlined in our previous study.[31] The concentrations of these biomarkers were determined using ELISA kits for CTX-1 (#E-EL-M3023, Elabscience, Wuhan, Hubei, China) and OCN (#E-EL-M0864c, Elabscience, Wuhan, Hubei, China) according to the instruction manual.

Immunofluorescence Staining

To evaluate the nuclear translocation of p65, immunofluorescence staining was performed. Briefly, BMMs were seeded onto sterile 12-well cover glasses at a density of 2×10^4 cells/cm² and cultured overnight. The cells were then pre-treated with either vehicle or 20 μM LBT for 4 h, followed by stimulation with 50 ng/mL RANKL for 0, 15, and 30 min. At the designated time points, cells were rinsed with PBS and fixed in 4% PFA for 10 min at RT. To minimize nonspecific background staining, fixed cells were incubated in PBS containing 1% BSA for 20 min. Subsequently, the cells were incubated overnight at 4°C with a rabbit anti-NF-κB p65 primary antibody (1:1000 dilution), followed by treatment with a Cy3-conjugated anti-rabbit secondary antibody (1:400 dilution) for 1 h at RT. Nuclei were counterstained with DAPI for 5 min at RT, and cells were mounted using an anti-fade medium. Fluorescent images of p65 localization were captured using the IXplore Standard Compound Microscope System (Olympus Corporation, Tokyo, Japan).

Statistical Analysis

Quantitative data were obtained from a minimum of five biological replicates, analyzed using GraphPad PRISM 8 (GraphPad Software, San Diego, CA, USA), and displayed as bar graphs or dot plots representing the mean ± standard deviation (SD). Statistical comparisons between groups were performed using Student's *t*-test, one-way ANOVA with Tukey's post hoc test. A p-value less than 0.05 was considered statistically significant, with significance levels indicated on the graphs by asterisks (*): $p < 0.05$ (*), $p < 0.01$ (**).

Results

Network Pharmacology Analysis of Lobetyolin and Osteoporosis

Using the SuperPred and Swiss Target Prediction databases, we identified 156 potential targets for LBT. From the GeneCards database, we retrieved 3629 osteoporosis-related targets based on the median relevance score. The overlap between LBT targets and osteoporosis-related targets was visualized through a Venn diagram, revealing 73 shared targets implicated in osteoporosis treatment (Figure 1A).

These 73 intersecting genes were further analyzed using the DAVID database for GO and KEGG pathway enrichment, with significance set at $p \leq 0.001$. GO analysis identified 51 enriched biological processes (BP), 12 cellular components (CC), and 11 molecular functions (MF). As shown in Supplementary Figure S1, prominent biological processes included the inflammatory response, positive regulation of cytosolic calcium ion concentration, and the ERK1/ERK2 cascade. Molecular functions were enriched for terms such as "nuclear receptor activity", "kinase activity", and "ATP binding", while cellular components predominantly involved the plasma membrane, cytoplasm, and the external side of the plasma membrane. Collectively, these results suggest that LBT's effects on osteoporosis are closely linked to these biological processes. KEGG pathway analysis highlighted 85 enriched pathways, with the top 20 visualized in Supplementary Figure S1. Key pathways associated with LBT's potential therapeutic effects included "Pathways in cancer" (hsa05200), "PI3K-Akt signaling pathway" (hsa04151), and "MicroRNAs in cancer" (hsa05206).

To further explore these findings, a network integrating LBT components, disease-related targets, and pathways was constructed using Cytoscape (Figure 1B). A protein-protein interaction (PPI) network of the enriched genes was developed through the STRING database, identifying core targets such as HSP90AA1 (degree: 34), EGFR (degree: 37), ESR1 (degree: 36), and NFKB1 (degree: 34) (Figure 1C).

Docking analysis was conducted using CB-DOCK2 software to evaluate the binding energy of LBT to these core targets. Binding energies below −1.2 kcal/mol (or −5 kJ/mol) were considered indicative of significant binding capacity. In our study, LBT exhibited binding energies below −5 kJ/mol for EGFR, ESR1, NFKB1, and HSP90AA1, suggesting spontaneous binding of the ligand to the receptor molecules. Among these, NFKB1 (binding energy: −5.7 kJ/mol) has been well-documented as a regulator in osteoporosis via the NF-κB signaling pathway, playing a critical role in suppressing inflammation, aging, and cancer.[32–35] Specific docking parameters for LBT and NFKB1 are detailed in Figure 1D.

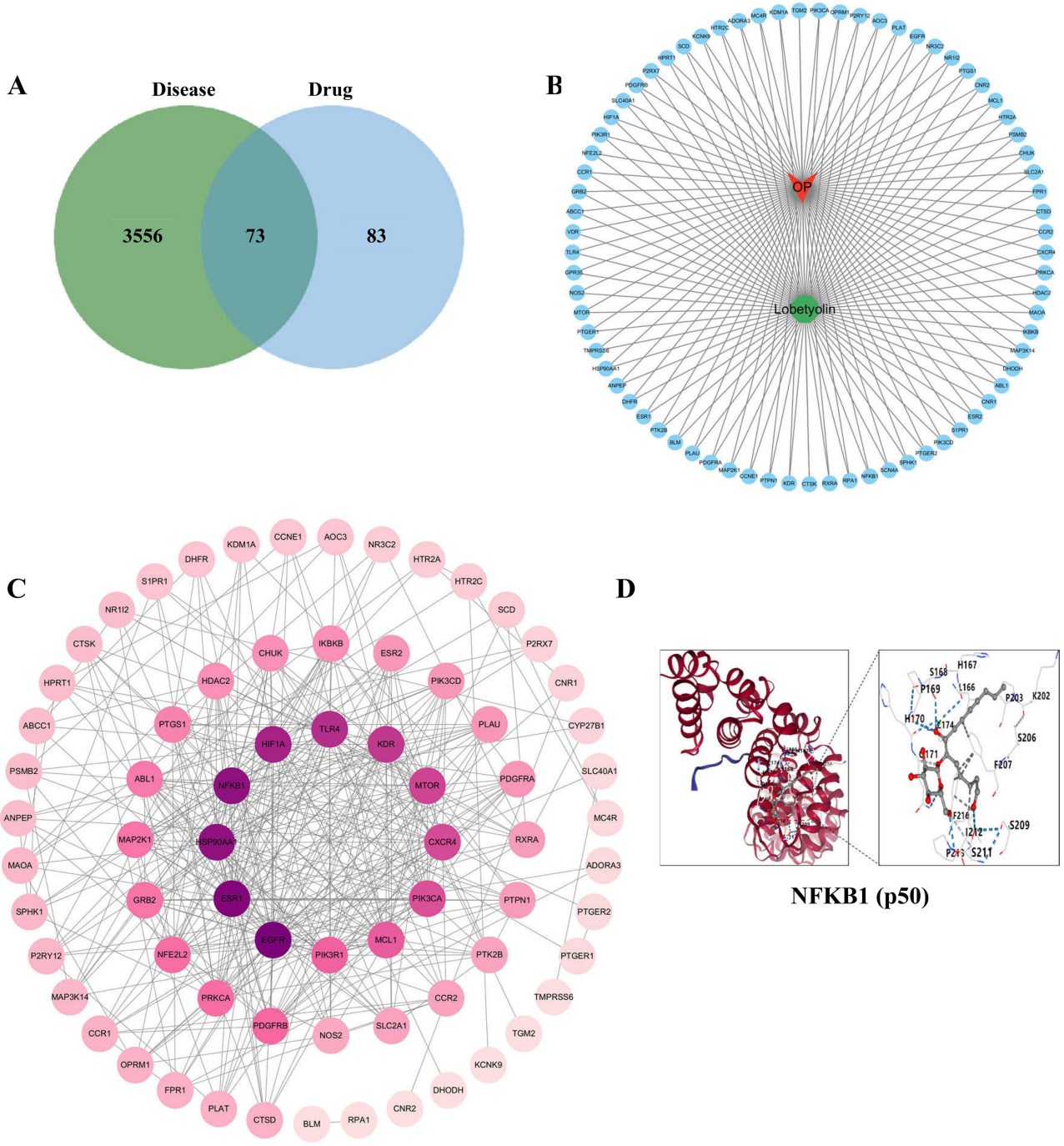

Figure 1 Network pharmacology analysis of lobetyolin and osteoporosis. (**A**) LBT-anti-osteoporosis disease target network diagram. (**B**) KEGG pathway analysis of LBT-anti -osteoporosis disease targets. (**C**) LBT-anti-osteoporosis disease PPI network. (**D**) Docking result of LBT with the NFKB1 (p50) target.

Lobetyolin Impeded Osteoclastogenesis and Osteoclast-Specific Gene Expression in vitro without Cytotoxicity

Upon identifying potential targets of LBT in the treatment of osteoporosis, we proceeded to evaluate its direct impact on osteoclast formation, a critical pathogenic factor in this condition. The condensed structural formula, molecular formula, and CAS number of LBT are presented in Figure 2A. Our initial focus was to assess the cytotoxic effects of LBT on BMM proliferation. According to the CCK-8 assay results, LBT at concentrations ranging from 0 to 20 μM exhibited no discernible cytotoxicity, even after 96 h of treatment. In contrast, higher concentrations (50–200 μM) displayed a dose-

https://doi.org/10.2147/DDDT.S515930

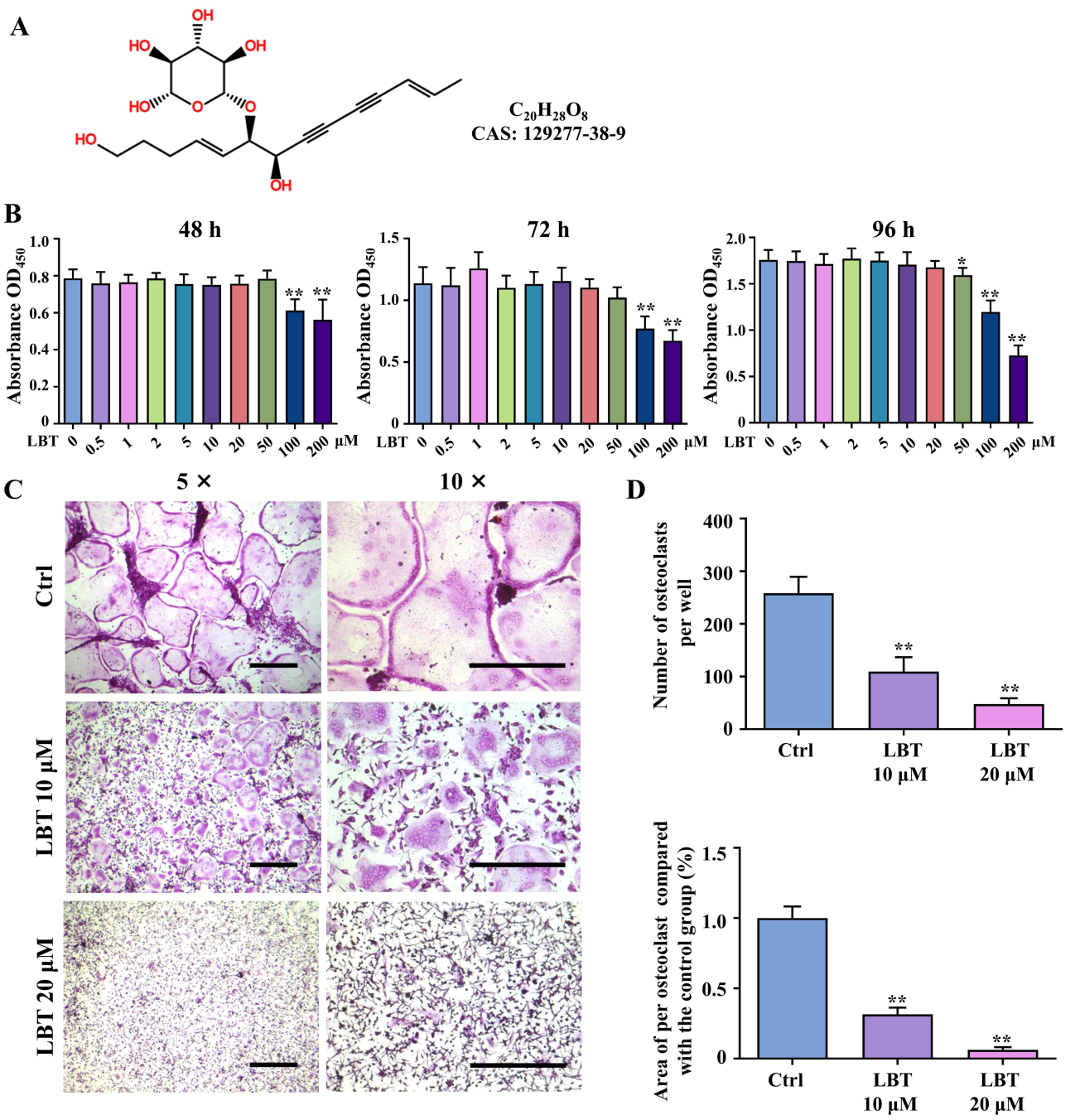

Figure 2 LBT dose-dependently inhibited RANKL-induced osteoclastogenesis without cytotoxicity in vitro. (**A**) The molecular structure, formula and CAS number of LBT. (**B**) BMMs were cultured with M-CSF in the presence of indicated concentrations of LBT for 48, 72 or 96 h, then cell viability was measured by cell counting kit-8 (n=6). (**C**) BMMs were stimulated with 30 ng/mL M-CSF and 50 ng/mL RANKL for 6 d and then subjected to TRAP staining. Scale bar, 400 μm. (**D**) Quantification of $TRAP^+$ multinucleated osteoclasts number and relative area per well (n=5). All values were presented as mean ± SD. *p<0.05, **p<0.01, relative to control group.

dependent inhibitory effect on cell viability (Figure 2B). Furthermore, we evaluated the toxicity of LBT via Calcein/PI fluorescence staining. As expected, the PI^+ cells were rarely detected in control, 10, and 20 μM LBT groups (Supplementary Figure S2). As a positive control, numerous PI^+ cells appeared in 100 μM LBT group.

Next, we investigated the influence of LBT on osteoclast differentiation. BMMs were seeded at a density of 5×10^4 cells per well in a 24-well plate, stimulated with RANKL, and treated with either a vehicle or increasing concentrations of LBT (10 and 20 μM) for 6 d, followed by TRAP staining. As depicted in Figure 2C, control group BMMs successfully differentiated into a substantial number of osteoclasts. However, LBT treatment significantly impeded osteoclastogenesis

in a dose-dependent manner. At 10 μM, LBT markedly reduced both the number and size of osteoclasts, while at 20 μM, osteoclast formation was almost entirely suppressed. Quantitative analysis revealed that TRAP-positive osteoclasts averaged 258.00 ± 31.48 per well in the control group, but decreased to 109.33 ± 27.39 and 47.67 ± 11.02 per well in the presence of 10 μM and 20 μM LBT, respectively. Similarly, the relative area of TRAP-positive osteoclasts was significantly smaller in LBT-treated groups compared to controls (Figure 2D). These findings highlight that LBT effectively suppresses osteoclastogenesis at non-cytotoxic concentrations.

As illustrated in Figure 3A, the addition of LBT during the early phase of osteoclast differentiation (days 0–2) significantly inhibited osteoclast formation. When LBT was introduced during the intermediate stage (days 2–4), the overall area covered by osteoclasts was noticeably reduced compared to the control group, although the total number of osteoclasts remained unchanged significantly. Similarly, administering LBT in the late stage of differentiation (days 4–6) resulted in the formation of smaller mature osteoclasts, without affecting their total count relative to the control (Figure 3B). These findings suggest that LBT primarily exerts its inhibitory effect on osteoclastogenesis during the early stage of differentiation.

To further elucidate the inhibitory effect of LBT on osteoclast differentiation, we performed qRT-PCR to evaluate the transcription levels of osteoclast-related genes in treated cells. The analysis revealed that LBT significantly down-regulated the expression of key genes associated with osteoclastogenesis in RANKL-stimulated BMMs, including *Nfatc1*, C-*fos, Ctsk, Dcstamp, Oscar, Acp5, Mmp9*, and *Calcr*, in a dose-dependent manner (Figure 3C–J).

Lobetyolin Suppressed Podosome Formation and Bone Resorption

Podosomes are highly dynamic, actin-rich structures that appear as small, dot-like formations within cells.[36] They are integral to processes such as adhesion, migration, and the degradation of the extracellular matrix.[37] In osteoclasts, podosomes are particularly essential, serving as key components that facilitate their bone-resorbing functions.[38] To investigate podosome formation in RANKL-treated BMMs, we employed phalloidin staining. FITC-phalloidin (green) was used to label podosomes, while DAPI (blue) was utilized to visualize nuclei. As depicted in Figure 4A and B, the control group displayed prominent green podosomes localized at the periphery of mature osteoclasts. However, treatment with 10 μM LBT led to a marked decrease in cell fusion and podosome formation, accompanied by reductions in nuclear count and cell size. Notably, at a concentration of 20 μM LBT, both cell fusion and podosome formation were almost entirely absent.

To evaluate the impact of LBT on osteoclast-mediated bone resorption, we conducted in vitro resorption assays. As illustrated in Figure 5A, osteoclasts treated with LBT exhibited markedly fewer and smaller resorption lacunae compared to the control group. Quantitatively, the relative number of bone resorption events decreased to 71.17 ± 11.87% and 26.17 ± 6.27% in the presence of 10 and 20 μM LBT, respectively (Figure 5B). Similarly, the relative area of bone resorption declined to 30.67 ± 8.34% and 13.00 ± 5.83% under the same treatment conditions. These findings collectively highlight the inhibitory effect of LBT on RANKL-induced podosome formation and osteoclastic bone resorption in vitro.

Furthermore, we detected ROS generation which is a characteristic during osteoclastogenesis and relative with inflammation via fluorescence staining. As expected, ROS generation was decreased in the 10 μM LBT group after 4 d RANKL stimulation, and almost entirely suppressed in the 20 μM LBT group (Figure 5C).

Lobetyolin Inhibited NFATc1, c-Fos, and Src Expression During Osteoclast Differentiation

To investigate the mechanism through which LBT suppresses osteoclastogenesis, we first analyzed its impact on the expression of c-Fos, NFATc1, and Src that were key transcriptional regulators and a protein kinase critical for osteoclast differentiation and activity. Western blot analysis revealed that, in the control group, RANKL stimulation of BMMs led to a time-dependent increase in c-Fos, NFATc1, and Src protein levels (Figure 6A). However, in the group treated with 20 μM LBT, the expression of these proteins was significantly reduced following RANKL compared to the control group. This finding was further corroborated by statistical analysis (Figure 6B).

In addition, the expression and nuclear translocation of NFATc1 were assessed through immunofluorescence co-localization. As shown in Figure 6C, a significant increase in NFATc1 expression and clear nuclear translocation were evident following 4 d RANKL induction. In contrast, LBT treatment notably inhibited this process.

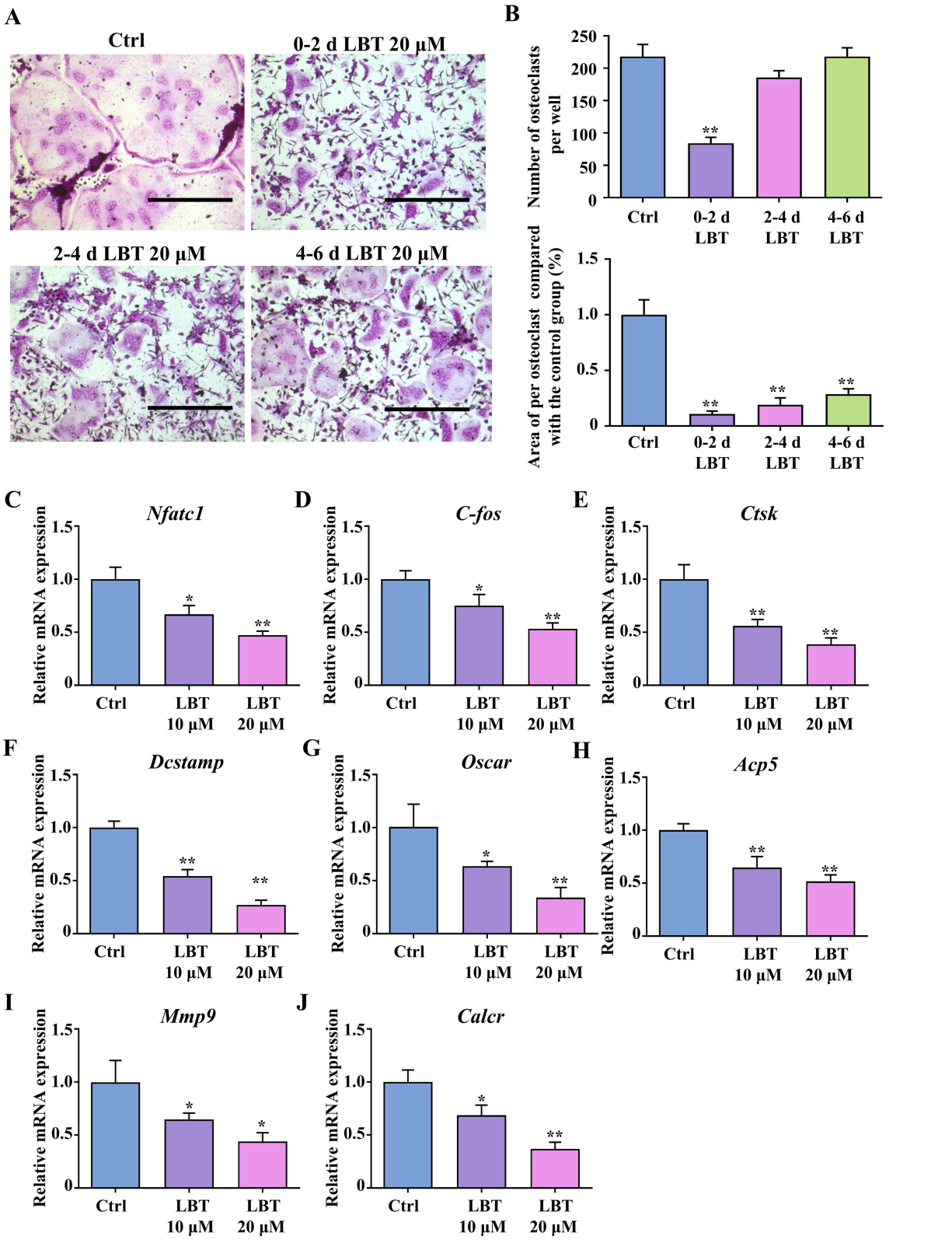

Figure 3 LBT primarily exerts its inhibitory effect on osteoclastogenesis on early stage and inhibited osteoclast-specific genes expression in vitro. (**A**) BMMs were stimulated with 30 ng/mL M-CSF for 6 d and 50 ng/mL RANKL for 0–2, 2–4, 4–6 d and then subjected to TRAP staining. Scale bar, 400 μm. (**B**) Quantification of $TRAP^+$ multinucleated osteoclasts number and relative area per well (n=5). (**C–J**) qPCR analysis of relative expression of the osteoclast-specific genes *Nfatc1* (**C**), *C-fos* (**D**), *Ctsk* (**E**), *Dcstamp* (**F**), *Oscar* (**G**), *Acp5* (**H**), *Mmp9* (**I**), and Calcr (**J**), in BMMs treated with RANKL and different concentrations of LBT (0, 10, and 20 μM) for 6 d. The relative changes in mRNA levels were analyzed by $2^{-\Delta\Delta CT}$ method. mRNA expression level of each target gene was first normalized to the expression of *GAPDH*, and then normalized to the control group (n=5). All values were presented as mean ± SD. *p<0.05, **p<0.01, relative to control group.

 https://doi.org/10.2147/DDDT.S515930

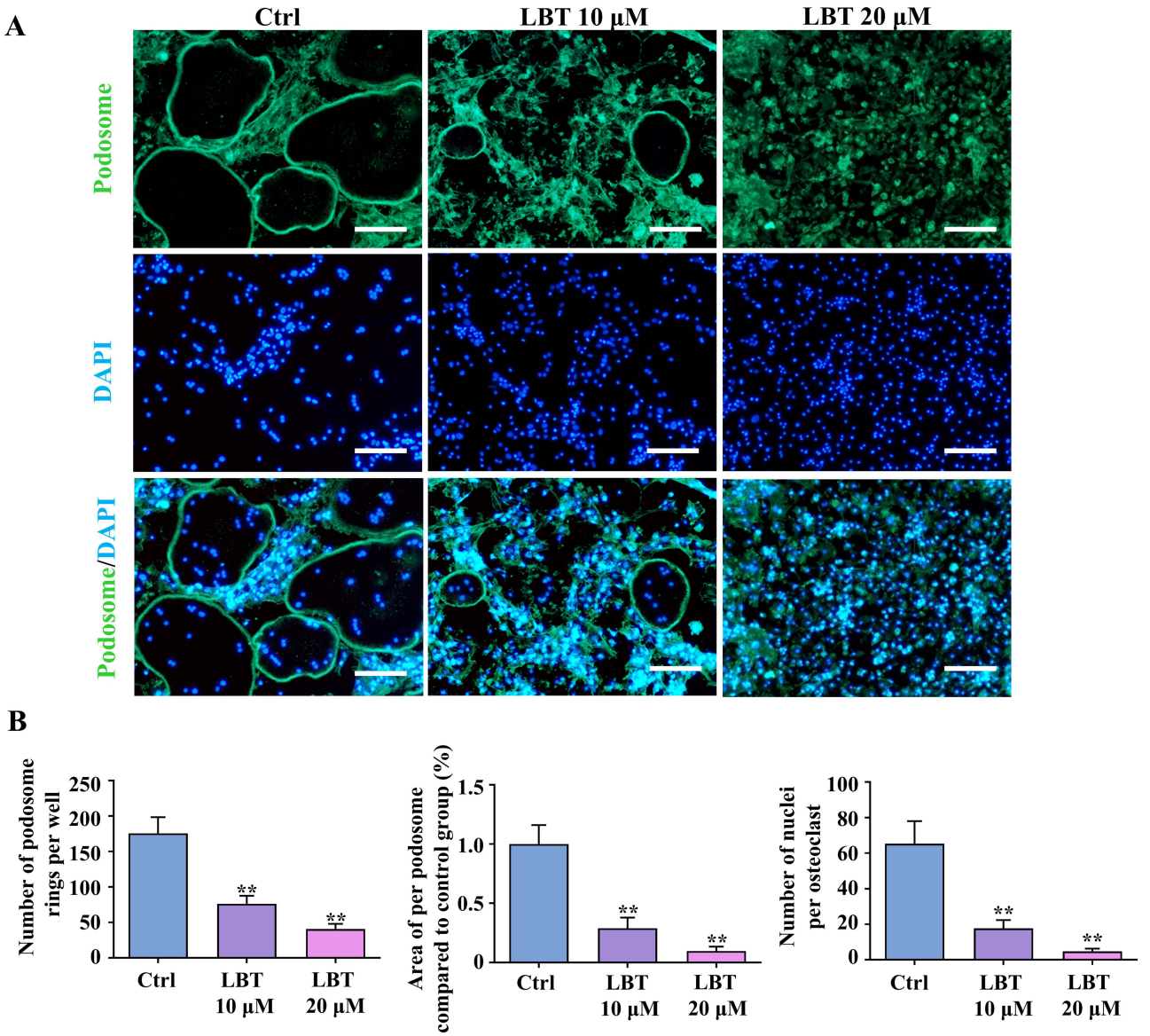

Figure 4 LBT inhibited RANKL-induced podosome formation in vitro. (**A**) Representative images of phalloidin staining of BMMs treated with RANKL and different concentrations of LBT (0, 10, or 20 μM) for 6 d. Green, podosome; Blue, nuclei. Scale bar, 200 μm. (**B**) Quantification of average number, relative area of podosomes per well and average number of nuclei per osteoclast (n=5). All values were presented as mean ± SD. **p<0.01, relative to control group.

Lobetyolin Restrained RANKL-Induced Activation of NF-κB Signaling Pathway

c-Fos and NFATc1, key transcriptional regulators in osteoclast differentiation, are modulated by various upstream signaling pathways, including MAPKs (p38, ERK, and JNK), NF-κB, and PI3K/AKT. To investigate their regulation, BMMs were pre-treated with either vehicle or 20 μM LBT for 4 h, followed by RANKL stimulation (50 ng/mL) for different time points (0, 5, 15, 30, or 60 min) prior to protein extraction. As shown in Figure 7A, phosphorylation of ERK, JNK, and p38, members of the MAPK family, peaked at 5, 15, and 5 min, respectively. Notably, no significant differences in the phosphorylation levels of these kinases were observed between the control and LBT-treated groups at these time points. Similarly, LBT had no noticeable effect on RANKL-induced AKT phosphorylation. However, LBT treatment markedly inhibited the phosphorylation of p65 at Ser536, a critical activation site within the NF-κB signaling pathway, at 5, 15, and 30 min post-RANKL stimulation (Figure 7B). These findings suggest that LBT may exert its inhibitory effects on osteoclastogenesis by disrupting NF-κB signaling and its downstream c-Fos/NFATc1 pathway.

https://doi.org/10.2147/DDDT.S515930

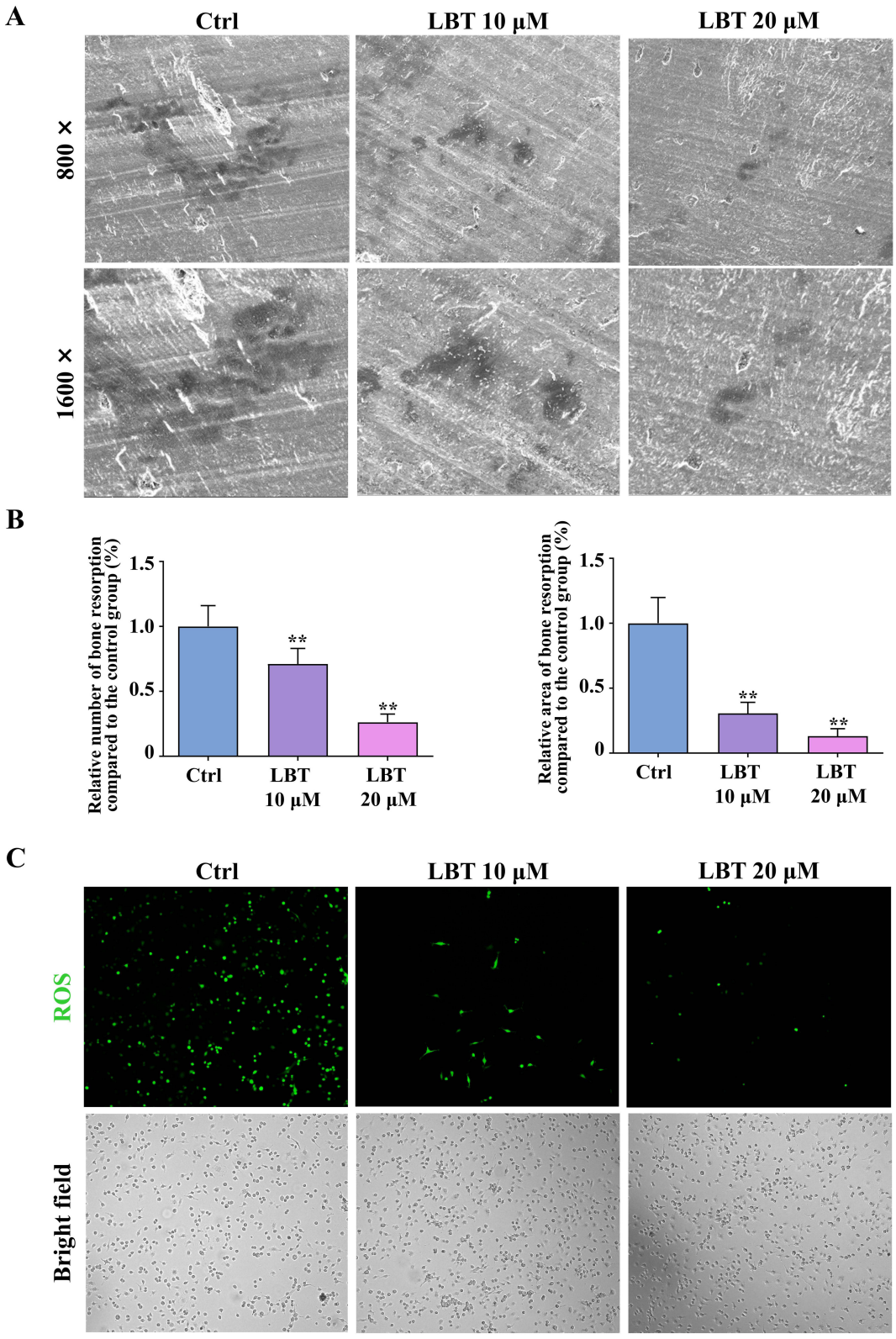

Figure 5 LBT suppressed osteoclastic bone resorption and ROS generation in vitro. (**A**) Representative scanning electron microscopy images of resorption pits on bovine slices planted with differentiating osteoclasts in the presence of 0, 10, or 20 μM LBT. (**B**) Quantification of number and relative area of bone resorption pits on SEM images (n=5). (**C**) Representative ROS fluorescence staining images of BMMs treated with RANKL and different concentrations of LBT (0, 10, or 20 μM) for 4 d. Green, ROS. All values were presented as mean ± SD. **p<0.01, relative to control group.

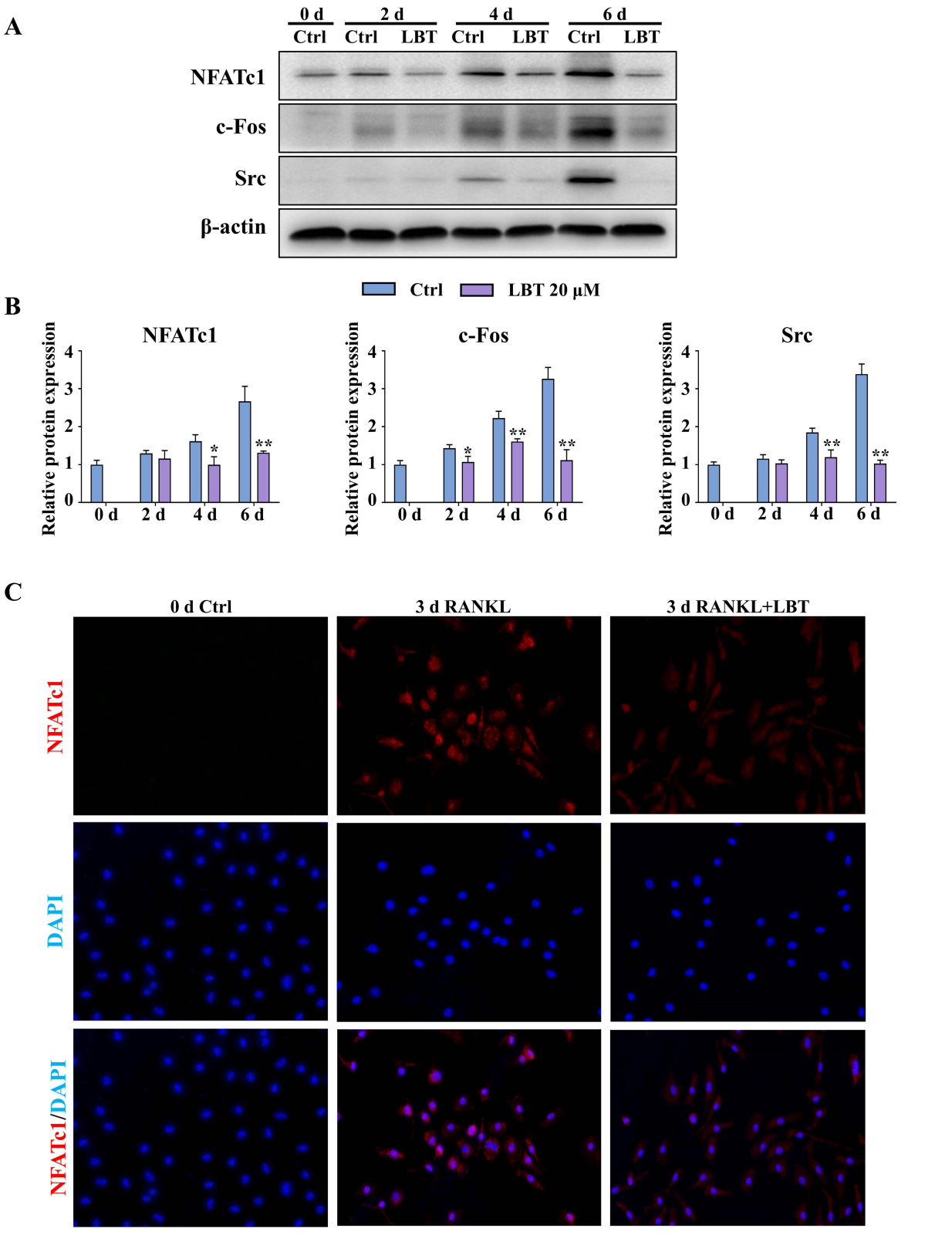

Figure 6 LBT suppressed NFATc1, c-Fos, and Src expression during osteoclastogenesis. (**A**) Western blot analyses of protein levels of NFATc1, c-Fos, and Src in the control or 20 μM LBT-treated BMMs at 0, 2, 4, and 6 d after RANKL stimulation. (**B**) Quantification of relative protein levels of NFATc1, c-Fos and Src in the control or 20 μM LBT-treated BMMs at 0, 2, 4, and 6 d after RANKL stimulation (n=5). (**C**) Representative NFATc1 immunofluorescent staining images of BMMs treated with RANKL and different concentrations of LBT (0, or 20 μM) for 4 d. All values were presented as mean ± SD. *p<0.05, **p<0.01, relative to control group on 0 d.

https://doi.org/10.2147/DDDT.S515930

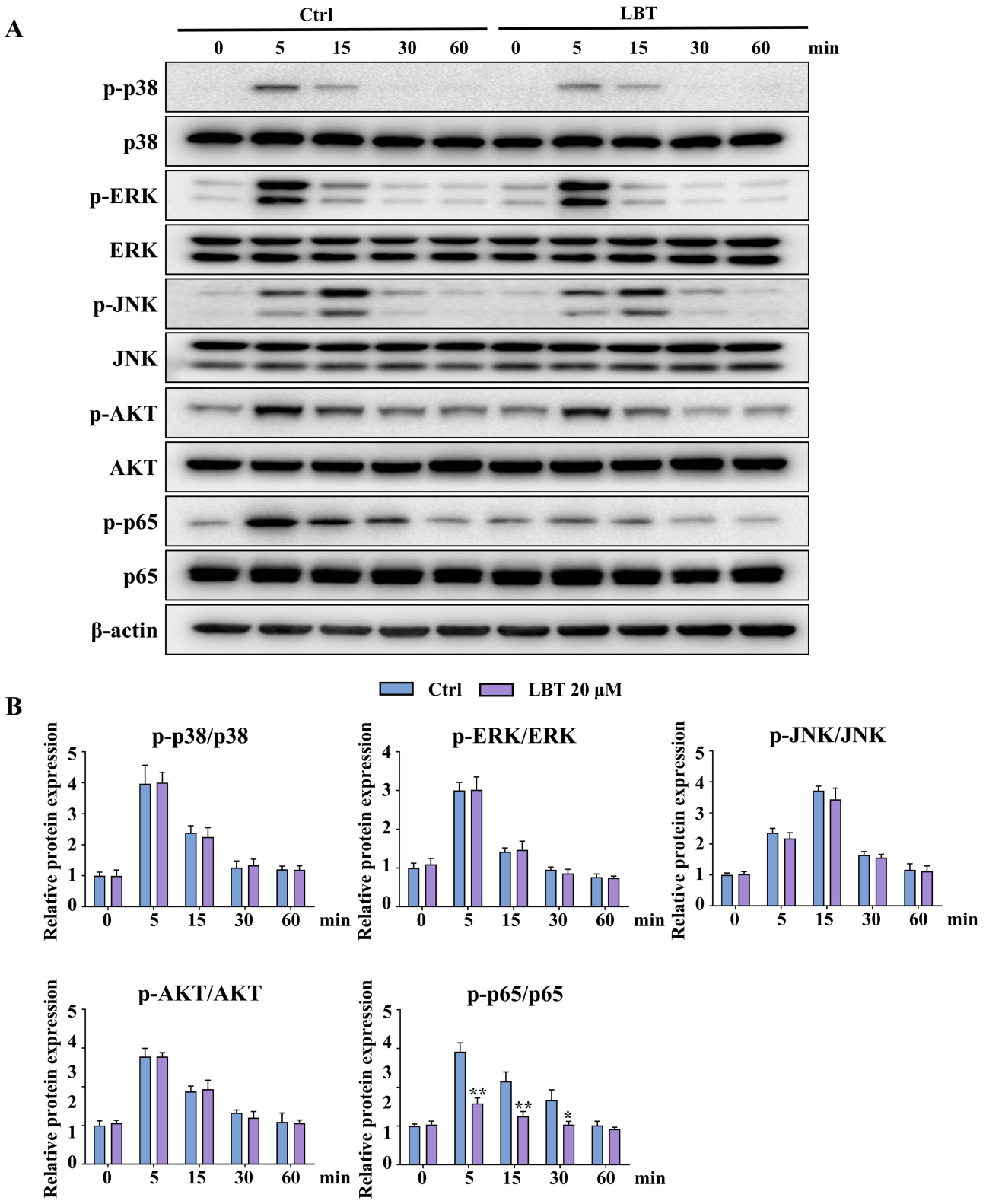

Figure 7 LBT inhibited NF-κB signaling pathway under RANKL stimulation. (**A**) Western blot analyses of protein levels of p-ERK/ERK, p-JNK/JNK and p-p38/p38, p-AKT/AKT and p-p65/p65 in BMMs treated with 50 ng/mL RANKL for indicate times in the presence of 0 or 20 μM LBT. (**B**) Quantification of relative protein levels of p-ERK/ERK, p-JNK/JNK and p-p38/p38, p-AKT/AKT and p-p65/p65 in the control or 20 μM LBT-treated BMMs treated with 50 ng/mL RANKL for indicate times (n=5). All values were presented as mean ± SD. *p<0.05, **p<0.01, relative to control group on 0 d.

 https://doi.org/10.2147/DDDT.S515930

To further investigate the involvement of NF-κB signaling in the mechanism by which LBT inhibits osteoclast differentiation, we examined the nuclear translocation of p65. Immunofluorescent staining revealed a pronounced translocation of p65 into the nucleus following 30 min RANKL stimulation (Figure 8A). As anticipated, pre-treatment with LBT effectively suppressed this nuclear translocation. Additionally, we analyzed the protein levels of p65 in both cytoplasmic and nuclear extracts from BMMs under the same treatment conditions. Consistent with the immunofluorescence results, Western blot analysis indicated that RANKL-induced nuclear translocation of p65 remained largely unchanged in LBT-treated BMMs compared to the control group (Figure 8B and C).

Lobetyolin Relieved LPS-Induced Osteogenesis Impairment

We previously had demonstrated that LBT suppressed osteoclast differentiation from BMMs under RANKL stimulation. Due to the fact that osteoclast-mediated bone resorption and osteoblast-mediated bone formation were essential for maintaining bone homeostasis, here we explored whether there was inhibitory effect of LBT on BMSCs proliferation. Firstly, we performed CCK-8 assays to assess the cytotoxic effect of LBT on BMSCs, the precursors of osteoblasts. Similar to its effect on BMMs, LBT treatment did not affect viability of BMSCs at lower concentrations (20 μM or below) within 96 h (Figure 9A).

In postmenopausal osteoporosis, a persistent inflammatory state within the bone marrow plays a central role in the disease's pathogenesis. This inflammation is often triggered by estrogen deficiency, immune cell activation, and an increase in the production of pro-inflammatory cytokines. Lipopolysaccharide (LPS), a molecular component of the outer membrane of Gram-negative bacteria, can activate immune cells and stimulate the release of various cytokines and intracellular signaling like NF-κB signaling, and is frequently utilized in osteoporosis research to induce a chronic inflammatory environment in the bone marrow, enabling the investigation of its impact on osteoblast differentiation. Subsequently, we examined the impact of 20 μM LBT on osteoblast differentiation under stimulation with 10 μg/mL LPS. Both ALP staining and Von Kossa staining demonstrated that LPS treatment significantly impaired alkaline phosphatase activity and calcium nodule formation during osteogenesis (Figure 9B and C). Notably, the addition of 20 μM LBT appeared to attenuate these inhibitory effects. Supporting these findings, qRT-PCR analysis further validated that LBT treatment partially reversed the suppression of osteoblast-specific gene transcription induced by LPS (Figure 9D–I).

Lobetyolin Protected Mice Against Ovariectomy-Induced Bone Loss

The aforementioned in vitro studies highlighted the protective effects of LBT in regulating osteoclast differentiation and mitigating LPS-induced osteogenic impairment. Building on these findings, we sought to investigate the potential of LBT in preventing postmenopausal osteoporosis using an in vivo model. For this purpose, ovariectomized (OVX) mice were employed as an animal model mimicking postmenopausal osteoporosis in women. Specifically, 8-week-old C57BL/6 mice underwent either OVX or sham surgeries and subsequently received daily intraperitoneal injections of vehicle or 20 mg/kg LBT, beginning three days post-surgery and continuing for five weeks. At the conclusion of the treatment period, the mice were euthanized for further analysis. To assess the impact of LBT on bone structure, trabecular bone at the distal femur was analyzed via μCT scanning. As anticipated, three-dimensional μCT reconstructions demonstrated that OVX intervention led to a significant decrease in trabecular bone mass beneath the femoral metaphysis in mice, which was effectively mitigated by LBT treatment (Figure 10A). Quantitative measurements further revealed that OVX significantly reduced trabecular bone volume fraction (BV/TV), trabecular number (Tb.N), and trabecular thickness (Tb.Th), while markedly increasing trabecular separation (Tb.Sp). Remarkably, these OVX-induced alterations were partially reversed in mice treated with LBT (Figure 10B–E). Serum levels of type I collagen cross-linked C-terminal peptide (CTX-1), a marker of bone resorption, and osteocalcin (OCN), a key indicator of bone formation, were measured using ELISA assays. Compared to the control group, OVX surgery resulted in a significant elevation of serum CTX-1 levels, which were notably reduced following LBT administration (Figure 10F), indicating an inhibitory effect of LBT on bone resorption. Meanwhile, the decline in serum OCN levels observed in OVX mice was partially restored by LBT treatment (Figure 10G).

Further histological assessments corroborated these findings. Both H&E and Von Kossa staining confirmed the protective effects of LBT against OVX-induced bone loss (Figure 11A). To explore whether the observed bone preservation was related to the suppression of osteoclast activity, TRAP staining was performed on femoral sections. OVX mice exhibited a substantial increase in the number of TRAP-positive multinucleated osteoclasts (N.Oc/BS) and

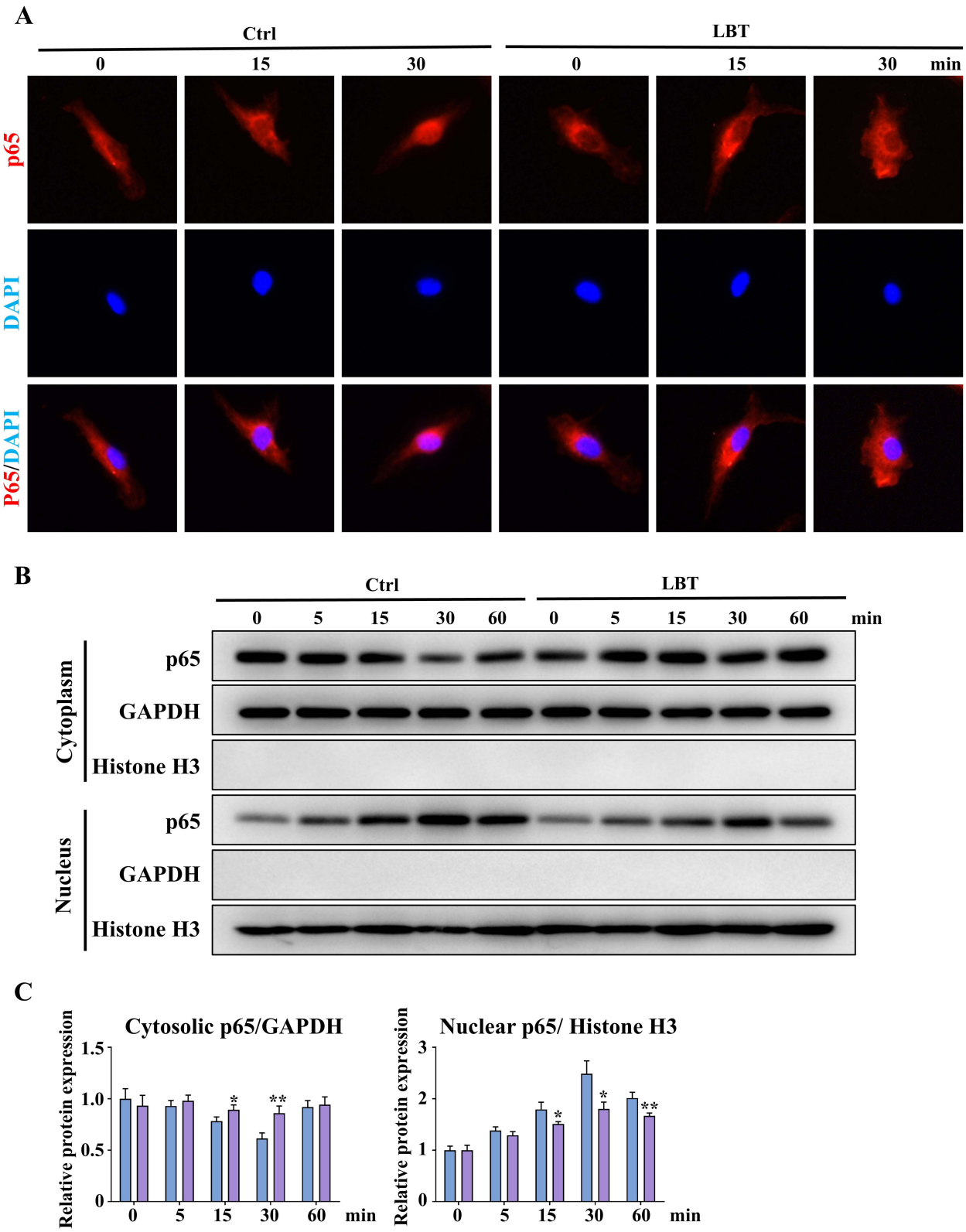

Figure 8 LBT hindered p65 nuclear translocation under RANKL stimulation. (**A**) Representative p65 immunofluorescent staining images of BMMs pre-treated with different concentrations of LBT (0, or 20 μM) and stimulated with RANKL for 0, 15, and 30 min. (**B**) Western blot analyses of protein levels of p65, GAPDH, and Histone H3 in cytoplasm and nucleus in BMMs treated with 50 ng/mL RANKL for indicate times in the presence of 0 or 20 μM LBT. (**C**) Quantification of relative protein levels of p65, GAPDH, and Histone H3 in cytoplasm and nucleus in BMMs treated with 50 ng/mL RANKL for indicate times in the presence of 0 or 20 μM LBT (n=5). All values were presented as mean ± SD. *p<0.05, **p<0.01, relative to control group on 0 d.

 https://doi.org/10.2147/DDDT.S515930

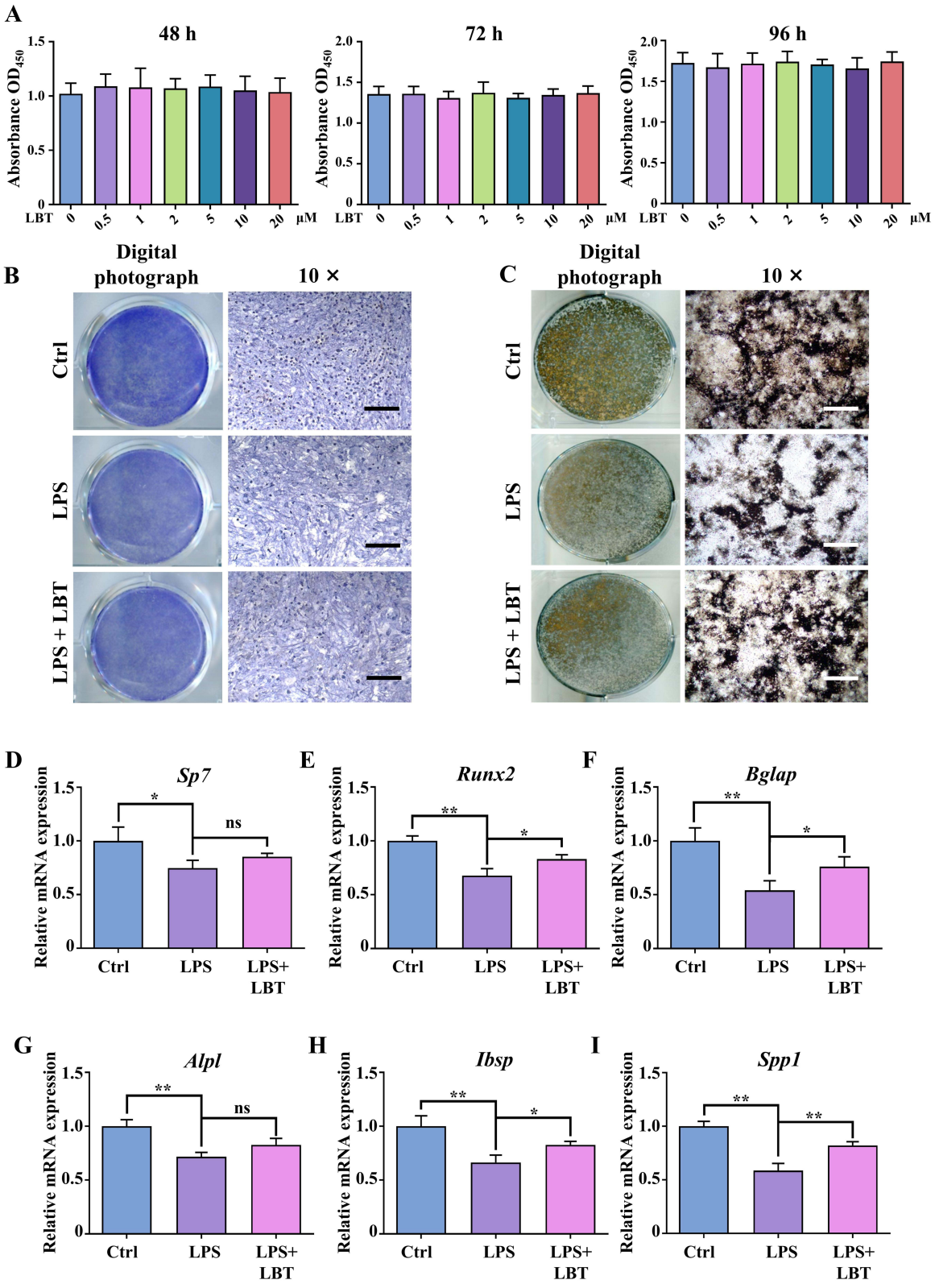

Figure 9 LBT relieved LPS-induced osteogenesis impairment. (**A**) BMSCs were cultured in the presence of indicated concentrations of LBT for 48, 72 or 96 h, then cell viability was measured by cell counting kit-8 (n=6). (**B**) BMSCs were stimulated with osteogenic induction with or without 10 μg/mL LPS or 20 μM LBT, and then subjected to ALP staining. Scale bar, 200 μm. (**C**) BMSCs were stimulated with osteogenic induction for 14 d with or without 10 μg/mL LPS or 20 μM LBT, and then subjected to Von Kossa staining. Scale bar, 200 μm. (**D–I**) qRT-PCR analysis of relative mRNA levels of osteoblast-specific genes, including *Sp7* (**D**), *Runx2* (**E**), *Bglap* (**F**), *Alpl* (**G**), *Ibsp* (**H**), *Spp1* (**I**), in BMSCs stimulated with osteogenic induction for 7 d with or without 10 μg/mL LPS or 20 μM LBT. The relative changes in mRNA levels were analyzed by $2^{-\Delta\Delta CT}$ method. mRNA expression level of each target gene was first normalized to the expression of *GAPDH*, and then normalized to the control group (n=5). All values were presented as mean ± SD. ns: not significant, *p<0.05, **p<0.01, determined by statistical analyses between two indicated groups.

https://doi.org/10.2147/DDDT.S515930

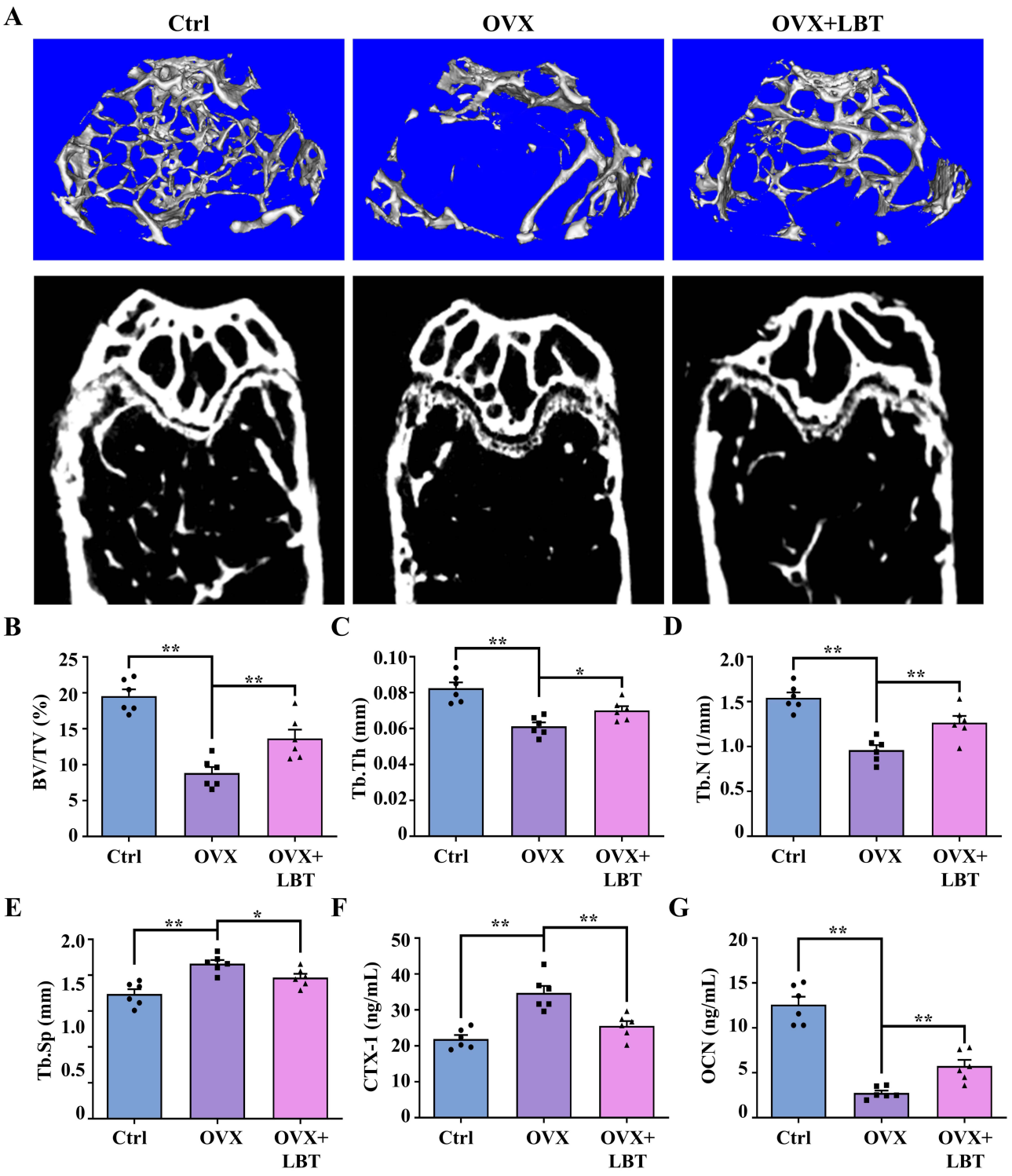

Figure 10 LBT alleviated bone loss in OVX mice. (**A**) Representative three-dimensional μCT images and coronal plane images of trabecular bones in the distal femurs from Ctrl, OVX, and OVX+LBT mice. White, bone (cancellous bone and cortical bone). (**B**–**E**) μCT analysis of the percentage of trabecular bone volume (BV/TV), trabecular number (Tb.N), trabecular thickness (Tb.Th), and trabecular separation (Tb.Sp) in the distal femurs (n-6). (**F**–**G**) Serum levels of bone resorption marker CTX-1 (**F**) and bone formation marker OCN (**G**) were determined by ELISA analysis (n=6). *p<0.05, **p<0.01, determined by statistical analyses between two indicated groups.

 https://doi.org/10.2147/DDDT.S515930

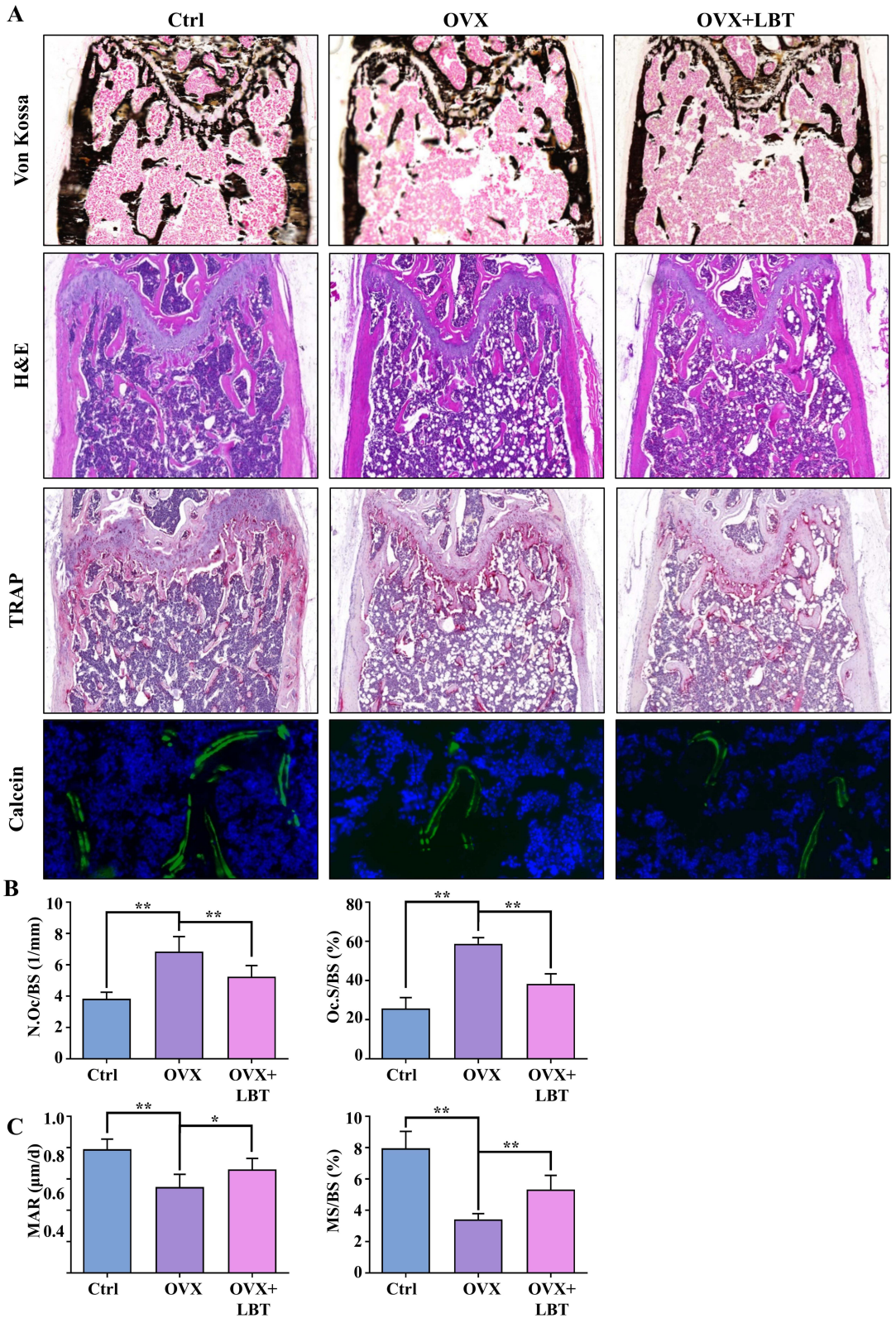

Figure 11 Histomorphometry analysis of distal femurs staining. (**A**) Representative images of distal femurs in Von Kossa, H&E, TRAP, and Calcein staining. (**B**) Histomorphometry analysis of number of OCs per trabecular bone surface (N. Oc/BS) and osteoclast surface per bone surface (Oc. S/BS) in TRAP staining images (n=6). (**C**) Histomorphometry analysis of mineral apposition rate (MAR) and mineralizing surface percentage (MS/BS) in calcein staining images (n=6). *p<0.05, **p<0.01, determined by statistical analyses between two indicated groups.

https://doi.org/10.2147/DDDT.S515930

the percentage of osteoclast surface relative to bone surface (Oc.S/BS), indicative of heightened osteoclastogenesis and resorption activity (Figure 11B). Strikingly, LBT treatment significantly attenuated these changes. Additionally, the impact of LBT on bone formation was examined. OVX surgery impaired osteogenesis along the trabecular surface, whereas LBT administration appeared to stimulate bone formation (Figure 11A). Bone histomorphometric analysis further validated the enhancement of osteoblast activity in LBT-treated mice (Figure 11C). At last, HE staining results of liver and myocardial tissues from three groups of mice in the OVX model demonstrated that no obvious long-term toxicity in vivo was founded during LBT treatment (Supplementary Figure S3). In summary, these findings demonstrate that LBT protects against OVX-induced bone loss by simultaneously inhibiting osteoclastogenesis and bone resorption, while promoting bone formation.

Discussion

Osteoporosis, particularly PMOP, remains a major global health concern, marked by diminished BMD, compromised bone microarchitecture, and a heightened risk of fractures. The onset and progression of this condition are largely driven by estrogen deficiency following menopause, which disrupts the delicate equilibrium between osteoclast-mediated bone resorption and osteoblast-driven bone formation.[39] This imbalance is further exacerbated by chronic inflammation, which not only accelerates osteoclast activity but also inhibits osteoblast function.[40,41] While existing pharmacological treatments, including bisphosphonates, denosumab, and teriparatide, offer therapeutic benefits, their prolonged use often leads to undesirable side effects, highlighting the urgent need for novel treatment approaches.[42] In light of this, our study explored the potential of LBT as a therapeutic strategy for PMOP, focusing on its effects on osteoclastogenesis, bone resorption, and osteoblast function. Through in vitro assays, we found that LBT, at low concentrations, exhibited no cytotoxicity and significantly suppressed osteoclast differentiation in a dose-dependent manner, resulting in a substantial decrease in osteoclast number and size. Moreover, LBT reduced the expression of osteoclast-specific genes and hindered podosome formation and bone resorption. Notably, LBT was shown to inhibit the activation of the NF-κB signaling pathway, a critical mediator of osteoclastogenesis. Additionally, LBT alleviated the osteogenesis impairment caused by LPS in BMSCs and facilitated osteoblast differentiation. In vivo, LBT offered protective effects against ovariectomy-induced bone loss in mice, as evidenced by improved bone structure, reduced osteoclast activity, and enhanced osteoblast function. Taken together, these findings suggest that LBT holds promise as a therapeutic agent for osteoporosis, capable of modulating osteoclast differentiation, inhibiting bone resorption, and promoting bone formation.

LBT is a bioactive compound primarily extracted from plants in the *Codonopsis pilosula*.[43,44] In recent years, it has garnered significant attention due to its promising pharmacological properties, including anti-inflammatory, anticancer, antioxidant, and neuroprotective effects.[45] While the precise molecular mechanisms of LBT's action remain incompletely understood, it is thought to exert its effects through modulation of various signaling pathways associated with oxidative stress, apoptosis, and inflammation.[46–49] LBT has been explored for its potential therapeutic applications in a variety of conditions. Its anti-inflammatory effects position it as a potential treatment for chronic diseases such as arthritis and inflammatory bowel disease.[49–51] Furthermore, its neuroprotective properties have led to investigations into its role in treating neurodegenerative disorders, including Alzheimer's diseases.[52] In the field of oncology, LBT is being studied as a possible adjunct to cancer therapy, given its ability to induce apoptosis (programmed cell death) in cancer cells.[53,54] Additionally, LBT has a long history of use in traditional medicine, particularly for treating respiratory illnesses.[55] Current research is focused on further elucidating its full spectrum of biological activities and optimizing its therapeutic potential, though further clinical trials are necessary to establish its safety and efficacy across different applications. In our study, network analysis identified several key targets, including HSP90AA1, EGFR, ESR1, and NFKB1, with docking studies revealing strong binding affinities between LBT and these targets. Notably, NFKB1 encodes a subunit (p50) of the NF-κB transcription factor, which is integral to regulating immune responses, inflammation, cell survival, and osteoclastogenesis.[56–58] While network pharmacology provides a powerful framework for identifying potential drug-target interactions and signaling pathways, its predictive outcomes are influenced by the quality and completeness of the databases used. This study suggests that the NF-κB signaling pathway may serve as a potential mechanism underlying the biological effects of LBT through network pharmacological analysis, which needs further molecular mechanism research. NF-κB signaling is triggered by various stimuli such as cytokines, stress, or pathogens, leading to the

phosphorylation and degradation of IκB proteins, which normally inhibit NF-κB. Once activated, NF-κB dimers (such as p65/p50) translocate to the nucleus, where they regulate the expression of genes involved in inflammation, immune responses, and cell survival.[59–61] In the context of osteoporosis, the NF-κB pathway enhances osteoclast differentiation and activity, promoting bone resorption.[62–64] Dysregulated NF-κB activity is strongly associated with excessive osteoclast activity and bone loss in osteoporosis. Pro-inflammatory cytokines including TNF-α and IL-6, which are elevated in osteoporosis, amplify NF-κB signaling, creating a feed-forward loop that exacerbates bone resorption.[65] NF-κB further induces the expression of transcription factors such as NFATc1, which drive osteoclast-specific gene programs.[66] This makes NF-κB a pivotal therapeutic target for mitigating pathological bone remodeling. By inhibiting this pathway, LBT may suppress osteoclastogenesis, offering a potential therapeutic approach for treating bone loss conditions.

NF-κB is typically composed of various dimers, including p65/p50, p50/p50, and RelB/p50. Among these, the p50 subunit plays a pivotal role in the canonical NF-κB signaling pathway, particularly in regulating inflammation and immune responses.[67–69] During osteoclastogenesis, p50 commonly forms dimers with p65 (RelA), which are the most transcriptionally active complexes upon RANKL stimulation. Activation of RANKL triggers the IKK complex (IκB kinase), leading to the phosphorylation and subsequent degradation of IκB proteins that normally sequester NF-κB dimers in the cytoplasm.[70] This degradation enables the translocation of p65/p50 dimers into the nucleus, where they initiate the transcription of genes critical for osteoclast differentiation, such as c-Fos, NFATc1, and other osteoclast-specific markers.[71–73] Additionally, the p50/p65 dimers promote the production of pro-inflammatory cytokines, such as TNF-α and IL-1, further amplifying the osteoclastogenic signaling cascade. Given that p50/p65 dimers are essential for the expression of key osteoclastogenic factors, the inhibition of p50 leads to a reduced expression of these factors, consequently impairing osteoclast differentiation. In mouse models with p50 deletion, a significant reduction in RANKL-induced osteoclastogenesis was observed. These mice demonstrated a decreased response to bone resorption signals and exhibited diminished trabecular bone loss, underscoring the crucial role of p50 in osteoclast differentiation and maintaining bone homeostasis.[74,75] Furthermore, in models of osteoporotic bone loss, p50 inhibition has been shown to protect against RANKL-induced osteoclastogenesis, highlighting its potential as a therapeutic target for osteoporosis and other bone-related diseases.[76]

However, While the findings provide valuable insights, certain limitations should be noted. Firstly, we fully acknowledge that the OVX mouse model, while widely validated for studying postmenopausal osteoporosis, does not fully recapitulate the complexity of human bone loss-related disease pathology. This model was selected due to its established utility in evaluating estrogen deficiency-induced bone loss and its alignment with standardized protocols for bone metabolism research.[77] However, we recognize that conclusions drawn from a single model may lack generalizability. Further researches may aim to validate LBT's therapeutic efficacy in complementary models (eg, aged mice or diabetic osteoporosis models), which will bridge preclinical and clinical translation. Secondly, based on previous literature reports and the results of network pharmacology in this study, we selected MAPKs (p38, JNK, ERK), AKT/PI3K and NF-κB signaling as potential mechanism research targets.[78,79] Although we have made it clear that LBT suppressed osteoclastogenesis via hindering NF-κB signaling not MAPKs and AKT/PI3K signal pathway, this cannot rule out the potential multi-target mechanism of LBT. The translational potential of LBT in clinical practice warrants careful consideration. Subsequently, the translational potential of LBT in clinical practice warrants careful consideration. Based on our mechanistic findings, several challenges must be addressed prior to clinical implementation such as pharmacokinetic optimization, long-term safety monitoring, and patient stratification. Emerging research areas such as the bone marrow microenvironment, macrophage polarization, ROS activation, and immune cell dysregulation are increasingly recognized as critical contributors to bone metabolism.[80–82] Due to space constraints, this study did not explore these mechanisms in depth. Future work will leverage advanced methodologies, including transcriptomics and single-cell omics, to systematically investigate these pathways.[83,84]

In the postmenopausal phase, the decline in estrogen levels triggers an elevation in the production of RANKL and a concomitant reduction in osteoprotegerin (OPG), a natural inhibitor of RANKL. This imbalance in the RANKL/OPG ratio fosters an overproduction of osteoclasts and excessive bone resorption.[85–87] The bone marrow microenvironment, which consists of diverse stromal cells, immune cells, and components of the extracellular matrix, plays a pivotal role in modulating local levels of RANKL and OPG, thereby influencing osteoclast differentiation and function. In the

postmenopausal state, estrogen deficiency triggers a cascade of events that not only disrupt the balance between osteoclasts and osteoblasts but also promote a pro-inflammatory environment in the bone marrow.[88,89] Inflammatory cytokines such as TNF-α, IL-1, and IL-6 are upregulated, contributing to the increased differentiation and activation of osteoclasts, which leads to enhanced bone resorption. This inflammatory milieu also impairs osteoblast function, further hindering bone formation and exacerbating bone loss.[90–93] Moreover, targeting specific inflammatory mediators may offer a novel approach to treat osteoporosis by not only addressing the inflammatory components but also enhancing the bone remodeling process.

Conclusion

In conclusion, our findings indicated that lobetyolin inhibited RANKL-induced osteoclast differentiation, fostered osteoblastogenesis under inflammatory environment in vitro, and safeguarded mice from OVX-induced osteoporosis in vivo by hindering p50/p65 nuclear translocation in the NF-κB signaling and modulating NFATc1/c-Fos expressions. These results position LBT as a potential therapeutic candidate for both preventing and treating OVX-related osteoporosis, as well as other bone disorders driven by excessive osteoclast activity. Future studies could explore the effects of LBT in additional osteoporosis models (eg, aging or glucocorticoid-induced bone loss) to validate its broader applicability. Further investigations into its pharmacokinetics, long-term safety, and synergistic potential with existing anti-osteoporotic therapies, as well as clinical trials to assess its efficacy in humans, will be critical steps toward translational application.

Abbreviations

PMOP, Postmenopausal osteoporosis; BMD, Bone mineral density; OBs, osteoblasts; OCs, Osteoclasts; BMMs, Bone marrow monocytes/macrophages; BMSCs, Bone marrow mesenchymal stromal cells; NF-κB, nuclear factor-κB; KEGG, Kyoto encyclopedia of genes and genomes; GO, gene ontology; PPI, protein-protein interaction; CCK-8, Cell counting kit-8; RANKL, Receptor activator for nuclear factor-κB ligand; M-CSF, Macrophage-colony stimulating factor; FBS, Fetal bovine serum; PMSF, Phenylmethanesulfonyl fluoride; LBT, Lobetyolin; DPBS, Dulbecco's phosphate-buffered saline; SPF, Specific pathogen-free; PI, Propidium iodide; RT, Room temperature; PFA, paraformaldehyde; F-actin, Filamentous actin; DAPI, 4′,6-diamidino-2-phenylindole dihydrochloride; BSA, Bovine serum albumin; SEM, Scanning electron microscope; ddH_2O, Double-distilled water; ROS, Reactive oxygen species; qRT-PCR, Quantitative reverse transcription-polymerase chain reaction; ALP, Alkaline phosphatase; μCT, Micro-computed tomography; ROI, Region of interest; VOI, Volume of interest; EDTA, Ethylenediaminetetraacetic acid; H&E, Hematoxylin and eosin; ELISA, Enzyme linked immunosorbent assay; LPS, Lipopolysaccharide; OVX, Ovariectomized; CTX-1, Type I collagen cross-linked C-terminal peptide; OCN, Osteocalcin; OPG, Osteoprotegerin.

Data Sharing Statement

Data will be made available on request.

Ethics Statement

The procedure was conducted in accordance with the Committee on the Ethics of Animal Experiments of Taizhou Hospital of Zhejiang Province (tzyy-2022007).

Funding

This work was supported by the National Natural Science Foundation of China (82202738), Natural Science Foundation of Zhejiang Province (LTGY24H250001), Taizhou Social Development Science and Technology project (22ywa06, 22ywb13), the Medical and Health Technology Program of Zhejiang Province (2023RC299), and Traditional Chinese Medicine Science and Technology Project of Zhejiang province (2024ZL194).

Disclosure

The authors declare that they have no known competing financial interests or personal relationships that could have appeared to influence the work reported in this paper.

References

1. Adejuyigbe B, Kallini J, Chiou D, Kallini JR. Osteoporosis: molecular pathology, diagnostics, and therapeutics. *Int J Mol Sci*. 2023;24(19):14583. doi:10.3390/ijms241914583
2. Foessl I, Dimai HP, Obermayer-Pietsch B. Long-term and sequential treatment for osteoporosis. *Nat Rev Endocrinol*. 2023;19(9):520–533. doi:10.1038/s41574-023-00866-9
3. Lu L, Tian L. Postmenopausal osteoporosis coexisting with sarcopenia: the role and mechanisms of estrogen. *J Endocrinol*. 2023;259(1). doi:10.1530/JOE-23-0116
4. Xie C, Jiang R, Wang C, Lei X, Lu K, Luo H. Development and validation of a nomogram integrating marital status for 5-year overall survival of chondrosarcoma: a population-based study. *Discov Oncol*. 2024;15(1):169. doi:10.1007/s12672-024-01020-1
5. Suzuki K. Chronic inflammation as an immunological abnormality and effectiveness of exercise. *Biomolecules*. 2019;9(6):223. doi:10.3390/biom9060223
6. Cosman F, Langdahl B, Leder BZ. Treatment sequence for osteoporosis. *Endocr Pract*. 2024;30(5):490–496. doi:10.1016/j.eprac.2024.01.014
7. Muñoz M, Robinson K, Shibli-Rahhal A. Bone health and osteoporosis prevention and treatment. *Clin Obstet Gynecol*. 2020;63(4):770–787. doi:10.1097/GRF.0000000000000572
8. Wu D, Li L, Wen Z, Wang G. Romosozumab in osteoporosis: yesterday, today and tomorrow. *J Transl Med*. 2023;21(1):668. doi:10.1186/s12967-023-04563-z
9. Ma L, Zhang L, Liao Z, et al. Pharmacological inhibition of protein S-palmitoylation suppresses osteoclastogenesis and ameliorates ovariectomy-induced bone loss. *J Orthop Transl*. 2023;42:1–14. doi:10.1016/j.jot.2023.06.002
10. Zhang L, Fu X, Ni L, et al. Hedgehog signaling controls bone homeostasis by regulating osteogenic/adipogenic fate of skeletal stem/progenitor cells in mice. *J Bone Miner Res*. 2022;37(3):559–576. doi:10.1002/jbmr.4485
11. Zhang L, Yang Y, Liao Z, et al. Genetic and pharmacological activation of Hedgehog signaling inhibits osteoclastogenesis and attenuates titanium particle-induced osteolysis partly through suppressing the JNK/c-Fos-NFATc1 cascade. *Theranostics*. 2020;10(15):6638–6660. doi:10.7150/thno.44793
12. Zhang L, Feng M, Li Z, et al. Bulleyaconitine A prevents Ti particle-induced osteolysis via suppressing NF-κB signal pathway during osteoclastogenesis and osteoblastogenesis. *J Cell Physiol*. 2018;233(9):7067–7079. doi:10.1002/jcp.26508
13. Tousen Y, Matsumoto Y, Nagahata Y, Kobayashi I, Inoue M, Ishimi Y. Resistant starch attenuates bone loss in ovariectomised mice by regulating the intestinal microbiota and bone-marrow inflammation. *Nutrients*. 2019;11(2):297. doi:10.3390/nu11020297
14. Piao J, Park JS, Hwang DY, Son Y, Hong HS. Substance P blocks ovariectomy-induced bone loss by modulating inflammation and potentiating stem cell function. *Aging*. 2020;12(20):20753–20777. doi:10.18632/aging.104008
15. Poulsen RC, Gotlinger KH, Serhan CN, Kruger MC. Identification of inflammatory and proresolving lipid mediators in bone marrow and their lipidomic profiles with ovariectomy and omega-3 intake. *Am J Hematol*. 2008;83(6):437–445. doi:10.1002/ajh.21170
16. Son HS, Lee J, Lee HI, et al. Benzydamine inhibits osteoclast differentiation and bone resorption via down-regulation of interleukin-1 β expression. *Acta Pharmaceutica Sinica B*. 2020;10(3):462–474. doi:10.1016/j.apsb.2019.11.004
17. Qiao S, Zhang X, Chen Z, Zhao Y, Tzeng CM. Alloferon-1 ameliorates estrogen deficiency-induced osteoporosis through dampening the NLRP3/caspase-1/IL-1β/IL-18 signaling pathway. *Int Immunopharmacol*. 2023;124(Pt B):110954. doi:10.1016/j.intimp.2023.110954
18. Chen S, Jin J, Xu Z, Han H, Wu L, Li Z. Catalpol attenuates osteoporosis in ovariectomized rats through promoting osteoclast apoptosis via the Sirt6-ERα-FasL axis. *Phytomedicine*. 2024;123:155262. doi:10.1016/j.phymed.2023.155262
19. Feng X, Liu Z, Su Y, et al. Tussilagone inhibits osteoclastogenesis by modulating mitochondrial function and ROS production involved Nrf2 activation. *Biochem Pharmacol*. 2023;218:115895. doi:10.1016/j.bcp.2023.115895
20. Wang J, Liu X, Wei W, et al. Regulation of oxygen-glucose deprivation/reperfusion-induced inflammatory responses and M1-M2 phenotype switch of BV2 microglia by lobetyolin. *Metab Brain Dis*. 2023;38(8):2627–2644. doi:10.1007/s11011-023-01292-6
21. Chen Z, Su Y, Ding J, He J, Lai L, Song Y. Lobetyolin protects mice against LPS-induced sepsis by downregulating the production of inflammatory cytokines in macrophage. *Front Pharmacol*. 2024;15:1405163. doi:10.3389/fphar.2024.1405163
22. Ma X, Zhao Y, Yang T, et al. Integration of network pharmacology and molecular docking to explore the molecular mechanism of Cordycepin in the treatment of Alzheimer's disease. *Front Aging Neurosci*. 2022;14:1058780. doi:10.3389/fnagi.2022.1058780
23. Shang L, Wang Y, Li J, et al. Mechanism of Sijunzi Decoction in the treatment of colorectal cancer based on network pharmacology and experimental validation. *J Ethnopharmacol*. 2023;302(Pt A):115876. doi:10.1016/j.jep.2022.115876
24. Tang B, Zhang X, Yang X, Wang W, Li R, Liu Y. Construction and validation of an angiogenesis-related scoring model to predict prognosis, tumor immune microenvironment and therapeutic response in hepatocellular carcinoma. *Front Immunol*. 2022;13:1013248. doi:10.3389/fimmu.2022.1013248
25. Xiong H, Guo H, Xie Y, et al. RNAseq analysis reveals pathways and candidate genes associated with salinity tolerance in a spaceflight-induced wheat mutant. *Sci Rep*. 2017;7(1):2731. doi:10.1038/s41598-017-03024-0
26. Nguyen VS, Loh XY, Wijaya H, et al. Specificity and inhibitory mechanism of andrographolide and its analogues as antiasthma agents on NF-κB p50. *J Natural Prod*. 2015;78(2):208–217. doi:10.1021/np5007179
27. Yoon IS, Cho SS. Effects of lobetyolin on xanthine oxidase activity in vitro and in vivo: weak and mixed inhibition. *Nat Prod Res*. 2021;35(10):1667–1670. doi:10.1080/14786419.2019.1622108
28. Ni SH, Zhang XJ, OuYang XL, et al. Lobetyolin alleviates ferroptosis of skeletal muscle in 5/6 nephrectomized mice via activation of Hedgehog-GLI1 signaling. *Phytomedicine*. 2023;115:154807. doi:10.1016/j.phymed.2023.154807
29. He W, Tao W, Zhang F, et al. Lobetyolin induces apoptosis of colon cancer cells by inhibiting glutamine metabolism. *J Cell Mol Med*. 2020;24(6):3359–3369. doi:10.1111/jcmm.15009

30. Yang Y, Liu Q, Zhang L, Fu X, Chen J, Hong D. A modified tape transfer approach for rapidly preparing high-quality cryosections of undecalcified adult rodent bones. *J Orthop Transl*. 2021;26:92–100. doi:10.1016/j.jot.2020.03.001
31. Cai G, Song X, Luo H, et al. NLRP3 blockade by MCC950 suppressed osteoclastogenesis via NF-κB/c-Fos/NFATc1 signal pathway and alleviated bone loss in diabetes mellitus. *Mol Cell Endocrinol*. 2024;594:112382. doi:10.1016/j.mce.2024.112382
32. Cartwright T, Perkins ND, Wilson CL. NFKB1: a suppressor of inflammation, ageing and cancer. *FEBS J*. 2016;283(10):1812–1822. doi:10.1111/febs.13627
33. Balla B, Kósa JP, Kiss J, et al. Different gene expression patterns in the bone tissue of aging postmenopausal osteoporotic and non-osteoporotic women. *Calcif Tissue Int*. 2008;82(1):12–26. doi:10.1007/s00223-007-9092-3
34. Balla B, Kósa JP, Kiss J, et al. Transcriptional profiling of immune system-related genes in postmenopausal osteoporotic versus non-osteoporotic human bone tissue. *Clin Immunol*. 2009;131(2):354–359. doi:10.1016/j.clim.2009.01.004
35. Nakamura H, Aoki K, Masuda W, et al. Disruption of NF-κB1 prevents bone loss caused by mechanical unloading. *J Bone Miner Res*. 2013;28(6):1457–1467. doi:10.1002/jbmr.1866
36. Dufrançais O, Mascarau R, Poincloux R, Maridonneau-Parini I, Raynaud-Messina B, Vérollet C. Cellular and molecular actors of myeloid cell fusion: podosomes and tunneling nanotubes call the tune. *Cell Mol Life Sci*. 2021;78(17–18):6087–6104. doi:10.1007/s00018-021-03875-x
37. Kong L, Wang B, Yang X, He B, Hao D, Yan L. Integrin-associated molecules and signalling cross talking in osteoclast cytoskeleton regulation. *J Cell Mol Med*. 2020;24(6):3271–3281. doi:10.1111/jcmm.15052
38. Chen ZH, Wu JJ, Guo DY, et al. Physiological functions of podosomes: from structure and function to therapy implications in osteoclast biology of bone resorption. *Ageing Res Rev*. 2023;85:101842. doi:10.1016/j.arr.2023.101842
39. Yao Y, Cai X, Chen Y, Zhang M, Zheng C. Estrogen deficiency-mediated osteoimmunity in postmenopausal osteoporosis. *Med Res Rev*. 2024;45(2):561–575. doi:10.1002/med.22081
40. Livshits G, Kalinkovich A. Targeting chronic inflammation as a potential adjuvant therapy for osteoporosis. *Life Sci*. 2022;306:120847. doi:10.1016/j.lfs.2022.120847
41. Zhang C, Li H, Li J, Hu J, Yang K, Tao L. Oxidative stress: a common pathological state in a high-risk population for osteoporosis. *Biomed Pharmacother*. 2023;163:114834.
42. ACOG Committee on Clinical Practice Guidelines–Gynecology. Management of postmenopausal osteoporosis: ACOG Clinical Practice Guideline No. 2. *Obstetrics Gynecol*. 2022;139(4):698–717. doi:10.1097/AOG.0000000000004730
43. Mu H, Jin Q, Tang J, Ye L, Wang B. Pharmacokinetics and related gender difference studies of four active components of Codonopsis Pilosula by LC-MS/MS determination. *J Ethnopharmacol*. 2025;337(Pt 2):118899. doi:10.1016/j.jep.2024.118899
44. Yue J, Xiao Y, Chen W. Insights into genus codonopsis: from past achievements to future perspectives. *Crit Rev Anal Chem*. 2024;54(8):3345–3376. doi:10.1080/10408347.2023.2242953
45. Bailly C. Anticancer properties of lobetyolin, an essential component of radix codonopsis (Dangshen). *Nat Prod Bioprospecting*. 2021;11(2):143–153. doi:10.1007/s13659-020-00283-9
46. Chen Y, Tian Y, Jin G, et al. Lobetyolin inhibits the proliferation of breast cancer cells via ASCT2 down-regulation-induced apoptosis. *Hum Exp Toxicol*. 2021;40(12):2074–2086. doi:10.1177/09603271211021476
47. Xie Q, Hu X, Zhao X, et al. Effects and mechanism of extracts rich in phenylpropanoids-polyacetylenes and polysaccharides from Codonopsis Radix on improving scopolamine-induced memory impairment of mice. *J Ethnopharmacol*. 2024;319(Pt 1):117106. doi:10.1016/j.jep.2023.117106
48. Cheng L, Zhai H, Du J, Zhang G, Shi G. Lobetyolin inhibits cell proliferation and induces cell apoptosis by downregulating ASCT2 in gastric cancer. *Cytotechnology*. 2023;75(5):435–448. doi:10.1007/s10616-023-00588-w
49. Chen G, Yang Y, Liu M, et al. Banxia xiexin decoction protects against dextran sulfate sodium-induced chronic ulcerative colitis in mice. *J Ethnopharmacol*. 2015;166:149–156. doi:10.1016/j.jep.2015.03.027
50. Chen Z, Zhou L, Ge Y, et al. Fuzi decoction ameliorates pain and cartilage degeneration of osteoarthritic rats through PI3K-Akt signaling pathway and its clinical retrospective evidence. *Phytomedicine*. 2022;100:154071. doi:10.1016/j.phymed.2022.154071
51. Liu C, Zhou M, Jiang W, et al. GPR105-targeted therapy promotes gout resolution as a switch between NETosis and apoptosis of neutrophils. *Front Immunol*. 2022;13:870183. doi:10.3389/fimmu.2022.870183
52. Zhao F, Fan L, Yang J, et al. Heterologous expression of BACE1 and its interaction with Codonopsis pilosula polysaccharides and Lobetyolin. *Int J Biol Macromol*. 2024;277(Pt 2):133440. doi:10.1016/j.ijbiomac.2024.133440
53. Hou YY, Qi SM, Leng J, et al. Lobetyolin, a Q-marker isolated from Radix Platycodi, exerts protective effects on cisplatin-induced cytotoxicity in HEK293 cells. *J Nat Med*. 2023;77(4):721–734. doi:10.1007/s11418-023-01714-w
54. Hu J, Wang D, Wang F, Lin P. Lobetyolin suppresses the proliferation of hepatocellular carcinoma through activating DUSP1-ERK1/2 signaling pathway. *Biol Pharm Bull*. 2024;47(10):1751–1758. doi:10.1248/bpb.b24-00307
55. Lu Y, Xu JY, Zhang XH, Zhao X. Gu-Ben-Fang-Xiao decoction attenuates sustained airway inflammation by suppressing ER stress response in a murine asthma remission model of respiratory syncytial virus infection. *J Ethnopharmacol*. 2016;192:496–509. doi:10.1016/j.jep.2016.09.039
56. Nurmi K, Silventoinen K, Keskitalo S, et al. Truncating NFKB1 variants cause combined NLRP3 inflammasome activation and type I interferon signaling and predispose to necrotizing fasciitis. *Cell Rep Med*. 2024;5(4):101503. doi:10.1016/j.xcrm.2024.101503
57. Chen TL, Tran M, Lakshmanan A, et al. NF-κB p50 (nfkb1) contributes to pathogenesis in the Eμ-TCL1 mouse model of chronic lymphocytic leukemia. *Blood*. 2017;130(3):376–379. doi:10.1182/blood-2017-01-761130
58. Novack DV. Role of NF-κB in the skeleton. *Cell Res*. 2011;21(1):169–182. doi:10.1038/cr.2010.159
59. Lawrence T. The nuclear factor NF-kappaB pathway in inflammation. *Cold Spring Harbor Perspect Biol*. 2009;1(6):a001651. doi:10.1101/cshperspect.a001651
60. Guo Q, Jin Y, Chen X, et al. NF-κB in biology and targeted therapy: new insights and translational implications. *Signal Transduct Target Ther*. 2024;9(1):53. doi:10.1038/s41392-024-01757-9
61. Cao Y, Yi Y, Han C, Shi B. NF-κB signaling pathway in tumor microenvironment. *Front Immunol*. 2024;15:1476030. doi:10.3389/fimmu.2024.1476030
62. Jiang T, Xia T, Qiao F, Wang N, Jiang Y, Xin H. Role and regulation of transcription factors in osteoclastogenesis. *Int J Mol Sci*. 2023;24(22):16175. doi:10.3390/ijms242216175
63. Yao Z, Getting SJ, Locke IC. Regulation of TNF-induced osteoclast differentiation. *Cells*. 2021;11(1):132. doi:10.3390/cells11010132

64. McDonald MM, Kim AS, Mulholland BS, Rauner M. New insights into osteoclast biology. *JBMR plus*. 2021;5(9):e10539. doi:10.1002/jbm4.10539
65. Soysa NS, Alles N. NF-kappaB functions in osteoclasts. *Biochem Biophys Res Commun*. 2009;378(1):1–5. doi:10.1016/j.bbrc.2008.10.146
66. Ilchovska DD, Barrow DM. An Overview of the NF-kB mechanism of pathophysiology in rheumatoid arthritis, investigation of the NF-kB ligand RANKL and related nutritional interventions. *Autoimmunity Rev*. 2021;20(2):102741. doi:10.1016/j.autrev.2020.102741
67. Barnabei L, Laplantine E, Mbongo W, Rieux-Laucat F, Weil R. NF-κB: at the borders of autoimmunity and inflammation. *Front Immunol*. 2021;12:716469. doi:10.3389/fimmu.2021.716469
68. Napetschnig J, Wu H. Molecular basis of NF-κB signaling. *Annu Rev Biophys*. 2013;42:443–468. doi:10.1146/annurev-biophys-083012-130338
69. DiDonato JA, Mercurio F, Karin M. NF-κB and the link between inflammation and cancer. *Immunol Rev*. 2012;246(1):379–400. doi:10.1111/j.1600-065X.2012.01099.x
70. Saito T, Tanaka S. Molecular mechanisms underlying osteoarthritis development: notch and NF-κB. *Arthritis Res Therapy*. 2017;19(1):94. doi:10.1186/s13075-017-1296-y
71. Peterson JM, Bakkar N, Guttridge DC. NF-κB signaling in skeletal muscle health and disease. *Curr Top Dev Biol*. 2011;96:85–119.
72. Mitchell S, Vargas J, Hoffmann A. Signaling via the NFκB system. *Wiley Interdiscip Rev Syst Biol Med*. 2016;8(3):227–241. doi:10.1002/wsbm.1331
73. Abu-Amer Y. NF-κB signaling and bone resorption. *Osteoporosis Int*. 2013;24(9):2377–2386. doi:10.1007/s00198-013-2313-x
74. Osorio FG, Soria-Valles C, Santiago-Fernández O, Freije JM, López-Otín C. NF-κB signaling as a driver of ageing. *Int Rev Cell Mol Biol*. 2016;326:133–174.
75. Tkach KE, Oyler JE, Altan-Bonnet G. Cracking the NF-κB code. *Sci Signaling*. 2014;7(313):pe5. doi:10.1126/scisignal.2005108
76. Courtois G, Smahi A. NF-kappaB-related genetic diseases. *Cell Death Differ*. 2006;13(5):843–851. doi:10.1038/sj.cdd.4401841
77. Komori T. Animal models for osteoporosis. *Eur J Pharmacol*. 2015;759:287–294. doi:10.1016/j.ejphar.2015.03.028
78. Yokota K. Osteoclast differentiation in rheumatoid arthritis. *Immunol Med*. 2024;47(1):6–11. doi:10.1080/25785826.2023.2220931
79. Agidigbi TS, Kim C. Reactive oxygen species in osteoclast differentiation and possible pharmaceutical targets of ROS-mediated osteoclast diseases. *Int J Mol Sci*. 2019;20(14):3576. doi:10.3390/ijms20143576
80. Li J, Chen X, Lu L, Yu X. The relationship between bone marrow adipose tissue and bone metabolism in postmenopausal osteoporosis. *Cytokine Growth Factor Rev*. 2020;52:88–98. doi:10.1016/j.cytogfr.2020.02.003
81. He X, Hu W, Zhang Y, et al. Cellular senescence in skeletal disease: mechanisms and treatment. *Cell Mol Biol Lett*. 2023;28(1):88. doi:10.1186/s11658-023-00501-5
82. Hu K, Shang Z, Yang X, Zhang Y, Cao L. Macrophage polarization and the regulation of bone immunity in bone homeostasis. *J Inflamm Res*. 2023;16:3563–3580. doi:10.2147/JIR.S423819
83. Mamidi N, Poellmann M, Javius-Jones K, Nam K, Hong S. Innovative hydrogel-based delivery systems for immunotherapy: a review of pre-clinical progress. *Nano Res*. 2024;17(10):9031–9043. doi:10.1007/s12274-024-6980-z
84. Madan E, Palma AM, Vudatha V, et al. Ovarian tumor cells gain competitive advantage by actively reducing the cellular fitness of microenvironment cells. *Nature Biotechnol*. 2024. doi:10.1038/s41587-024-02453-3
85. Azizieh FY, Shehab D, Jarallah KA, Gupta R, Raghupathy R. Circulatory levels of RANKL, OPG, and oxidative stress markers in postmenopausal women with normal or low bone mineral density. *Biomarker Insights*. 2019;14:1177271919843825. doi:10.1177/1177271919843825
86. Cheng CH, Chen LR, Chen KH. Osteoporosis due to hormone imbalance: an overview of the effects of estrogen deficiency and glucocorticoid overuse on bone turnover. *Int J Mol Sci*. 2022;23(3):1376.
87. Ni X, Wu B, Li S, et al. Equol exerts a protective effect on postmenopausal osteoporosis by upregulating OPG/RANKL pathway. *Phytomedicine*. 2023;108:154509. doi:10.1016/j.phymed.2022.154509
88. Jochems C, Islander U, Erlandsson M, Verdrengh M, Ohlsson C, Carlsten H. Osteoporosis in experimental postmenopausal polyarthritis: the relative contributions of estrogen deficiency and inflammation. *Arthritis Res Therapy*. 2005;7(4):R837–843. doi:10.1186/ar1753
89. Ali D, Figeac F, Caci A, et al. High-fat diet-induced obesity augments the deleterious effects of estrogen deficiency on bone: evidence from ovariectomized mice. *Aging Cell*. 2022;21(12):e13726. doi:10.1111/acel.13726
90. Fischer V, Haffner-Luntzer M. Interaction between bone and immune cells: implications for postmenopausal osteoporosis. *Semin Cell Dev Biol*. 2022;123:14–21. doi:10.1016/j.semcdb.2021.05.014
91. McLean RR. Proinflammatory cytokines and osteoporosis. *Curr Osteoporosis Rep*. 2009;7(4):134–139. doi:10.1007/s11914-009-0023-2
92. Lacativa PG, Farias ML. Osteoporosis and inflammation. *Arquivos brasileiros de endocrinologia e metabologia*. 2010;54(2):123–132. doi:10.1590/S0004-27302010000200007
93. Brincat SD, Borg M, Camilleri G, Calleja-Agius J. The role of cytokines in postmenopausal osteoporosis. *Minerva Ginecologica*. 2014;66(4):391–407.